ARTICLE

IFNγ-activated dermal lymphatic vessels inhibit cytotoxic T cells in melanoma and inflamed skin

Ryan S. Lane[1], Julia Femel[1], Alec P. Breazeale[1], Christopher P. Loo[1], Guillaume Thibault[2,3], Andy Kaempf[4], Motomi Mori[4], Takahiro Tsujikawa[1,5], Young Hwan Chang[2,3], and Amanda W. Lund[1,3,6,7,8]

Mechanisms of immune suppression in peripheral tissues counteract protective immunity to prevent immunopathology and are coopted by tumors for immune evasion. While lymphatic vessels facilitate T cell priming, they also exert immune suppressive effects in lymph nodes at steady-state. Therefore, we hypothesized that peripheral lymphatic vessels acquire suppressive mechanisms to limit local effector CD8+ T cell accumulation in murine skin. We demonstrate that nonhematopoietic PD-L1 is largely expressed by lymphatic and blood endothelial cells and limits CD8+ T cell accumulation in tumor microenvironments. IFNγ produced by tissue-infiltrating, antigen-specific CD8+ T cells, which are in close proximity to tumor-associated lymphatic vessels, is sufficient to induce lymphatic vessel PD-L1 expression. Disruption of IFNγ-dependent crosstalk through lymphatic-specific loss of IFNγR boosts T cell accumulation in infected and malignant skin leading to increased viral pathology and tumor control, respectively. Consequently, we identify IFNγR as an immunological switch in lymphatic vessels that balances protective immunity and immunopathology leading to adaptive immune resistance in melanoma.

Introduction

Lymphatic vessels compose a hierarchical vasculature that facilitates the unidirectional transport of fluid and cells from peripheral, blind-ended capillaries through collecting vessels to lymphatic sinuses in secondary lymphoid organs (Stacker et al., 2014). Lymphatic vessels transport antigen and dendritic cells (DCs) to LNs to prime naive T cells following peripheral tissue viral infection (Allan et al., 2006; Bedoui et al., 2009; Loo et al., 2017) and remain the main route of DC migration and de novo immune priming in tumors (Lund et al., 2016b; Roberts et al., 2016). Consistent with the role for lymphatic vessels in de novo adaptive immunity, lymphatic vessel density (LVD) in primary tumors of colorectal patients positively correlates with intratumoral CD8+ T cell infiltrates (Mlecnik et al., 2016; Bordry et al., 2018), and similarly, work in mouse models demonstrates a causal relationship between tumor-associated lymphangiogenesis and intratumoral inflammation (Lund et al., 2012, 2016b; Alitalo et al., 2013; Fankhauser et al., 2017) leading to improved response to immunotherapy (Fankhauser et al., 2017). Thus, lymphatic transport shapes inflammatory and immune microenvironments in solid tumors (Lund, 2016).

Rather than acting as passive conduits, however, lymphatic capillaries are responsive to their inflamed tissue microenvironment (Vigl et al., 2011) and remodeled in infected, inflamed, and neoplastic tissue (Lund et al., 2016a). In infected skin, type I IFN remodels lymphatic capillaries and rapidly shuts down fluid transport leading to viral sequestration (Loo et al., 2017); sustained inflammation following *Yersinia pseudotuberculosis* infection induces collecting lymphatic vessel leakage leading to insufficient DC migration to LNs and poor immunity (Fonseca et al., 2015); and lymphatic transport is elevated from tumors early, before metastatic seeding (Ruddell et al., 2015), but decreases with tumor progression (Rohner et al., 2015). Furthermore, lymphatic endothelial cells (LECs) are activated by inflammatory cytokines and elevated interstitial fluid flows, increasing expression of chemokines and adhesion molecules necessary for DC trafficking (Johnson et al., 2006; Miteva et al., 2010). Consequently, peripheral lymphatic capillaries tune their transport function (fluid and cellular) in response to inflammatory cues with functional consequences for tissue inflammation and immunity.

[1]Department of Cell, Developmental and Cancer Biology, Oregon Health and Science University, Portland, OR; [2]Department of Biomedical Engineering and Computational Biology Program, Oregon Health and Science University, Portland, OR; [3]OHSU Center for Spatial Systems Biomedicine, Oregon Health and Science University, Portland, OR; [4]Knight Cancer Institute, Biostatistics Shared Resource, Oregon Health and Science University, Portland, OR; [5]Department of Otolaryngology-Head and Neck Surgery, Kyoto Prefectural University of Medicine, Kyoto City, Kyoto, Japan; [6]Department of Molecular Microbiology and Immunology, Oregon Health and Science University, Portland, OR; [7]Department of Dermatology, Oregon Health and Science University, Portland, OR; [8]Knight Cancer Institute, Oregon Health and Science University, Portland, OR.

Correspondence to Amanda W. Lund: lunda@ohsu.edu.

Interestingly, beyond their bulk transport properties, LECs that compose lymphatic sinuses in LNs exhibit unique, intrinsic immunological activity that can both facilitate and suppress adaptive immune responses. In vaccine models, LN LECs scavenge and archive antigen to support future memory responses (Tamburini et al., 2014), while in tumor-draining LNs (tDLNs), LECs, rather, cross-present scavenged tumor antigens leading to dysfunctional T cell priming (Lund et al., 2012; Hirosue et al., 2014). Furthermore, at steady-state, LECs constitutively express the coinhibitory molecule programmed death-ligand 1 (PD-L1) and maintain CD8^{+} T cell tolerance through Aire-independent, promiscuous expression of peripheral tissue antigens (Cohen et al., 2010; Tewalt et al., 2012) and inhibit T cell proliferation through production of nitric oxide (Lukacs-Kornek et al., 2011). Thus, LN LECs are thought to be critical players in the maintenance of peripheral tolerance to self-antigen, specifically within the unique microenvironment of LNs at steady-state (Cohen et al., 2010, 2014; Lukacs-Kornek et al., 2011; Tewalt et al., 2012; Rouhani et al., 2015). Whether the LECs that compose lymphatic capillaries in peripheral, nonlymphoid tissues acquire similar functionality, however, is unclear. Two reports indicate that tissue inflammation induces PD-L1 expression on LECs in skin (Vigl et al., 2011) and orthotopic, implanted tumors (Dieterich et al., 2017), suggesting that peripheral LECs may acquire similar immunological function. The functional relevance of peripheral LEC PD-L1 expression in vivo, however, remains unknown.

Tumors use multiple mechanisms to evade host immunity, including the expression of coinhibitory molecules, such as PD-L1, that limit T cell effector function in tumor microenvironments. Melanoma exhibits robust responses to immune checkpoint blockade as a result of significant CTL infiltrates that secrete IFNγ and activate expression of PD-L1 in tumors (Spranger et al., 2013). This phenomenon, termed adaptive immune resistance (Ribas, 2015), protects tumor cells from CTL-mediated killing through PD-L1–dependent inhibition of TCR signaling (Juneja et al., 2017). In addition to PD-L1 expression by tumor cells, however, recent work highlights the role of host hematopoietic cells in PD-L1–dependent T cell exhaustion in mouse (Lin et al., 2018; Tang et al., 2018) and human studies (Herbst et al., 2014), indicating that tumor microenvironments contribute to CTL exhaustion. Importantly, in nonmalignant settings, expression of PD-L1 by host cells serves to protect tissue from excessive immune-mediated damage and mediate return to homeostasis (Mueller et al., 2010; Frebel et al., 2012), and nonhematopoietic cells play a key tissue-protective role in chronic inflammation (Scandiuzzi et al., 2014) and chronic viral infection (Mueller et al., 2010; Frebel et al., 2012). The functional significance of a nonhematopoietic PD-L1 source in tumors, however, has not been demonstrated.

Herein we demonstrate that peripheral lymphatic vessels are exquisite sensors of interstitial IFNγ in tumor and inflamed microenvironments and initiate immune suppressive programs that functionally limit the further accumulation of CTLs. At least one component of this response is expression of PD-L1, and we demonstrate that nonhematopoietic cells contribute to local, PD-L1–dependent, effector CD8^{+} T cell control. Importantly, we demonstrate that, when lacking IFNγR, peripheral lymphatic vessels fail to express PD-L1 in response to CTL infiltration, and

as a consequence, CTL function in tumor microenvironments is improved. Thus, using both acute cutaneous viral models and multiple tumor models, we demonstrate that lymphatic vessels balance protective CD8^{+} effector T cell immunity and immunopathology and identify the tumor-associated lymphatic vasculature as a critical component of tumor microenvironment–mediated control of effector, anti-tumor immunity.

Results

Nonhematopoietic PD-L1 limits the accumulation of cytotoxic CD8^{+} T cells in melanoma

Immune checkpoint blockade, including antibodies targeted against PD-L1, is achieving unprecedented clinical responses (Topalian et al., 2012; Wolchok et al., 2013; Herbst et al., 2014). The toxicity associated with treatment, however, necessitates the identification of predictive biomarkers that would target a patient population most likely to respond. Though patients with PD-L1^{+} tumor cells are enriched for responders, PD-L1[–] patients also respond (Robert et al., 2015; Ribas et al., 2016), indicating that additional cellular players and potentially other anatomical locations contribute to patient response and should be explored further. Recent work highlights the role of host and, in particular, hematopoietic, PD-L1 expression in tumor-associated T cell exhaustion in mice (Lin et al., 2018; Tang et al., 2018) and stratification of patient response in humans (Herbst et al., 2014); however, whether nonhematopoietic, nontumor sources of PD-L1 additionally contribute to intratumoral mechanisms of T cell control remains unexplored. Importantly, nonhematopoietic expression of PD-L1 contributes to immunopathology during chronic viral infection (Mueller et al., 2010) and DSS-induced colitis (Scandiuzzi et al., 2014), and PD-L1 expression by LN LECs maintains peripheral tolerance at steady-state (Tewalt et al., 2012). We therefore asked whether PD-L1 expressed by nontumor, nonhematopoietic stromal cells functionally inhibits CD8^{+} T cell responses within tumor microenvironments. To ask this question, we generated PD-L1^{−/−} bone marrow chimeras by lethal irradiation of WT or PD-L1^{−/−} mice and reconstitution with either WT or PD-L1^{−/−} bone marrow (reconstitution >80%; Fig. 1 A). B16F10 tumors were implanted in reconstituted mice and analyzed at endpoint. While there was no significant change in tumor growth compared with controls (Fig. 1 B), consistent with the poor sensitivity of B16F10 tumors to single agent PD-L1 blockade (Kleffel et al., 2015), both hematopoietic and nonhematopoietic chimeras accumulated more activated CD44^{+} CD8^{+} T cells (Fig. 1 C) with increased expression of the effector molecule PD-1 (Fig. 1 D) and the core-2 O-linked glycosylation motif required for effector trafficking (1B11; Fig. 1 E; Nolz and Harty, 2014), demonstrating that PD-L1 expressed by both tumor-infiltrating leukocytes and tumor-resident, nonhematopoietic stromal cells limits effector CD8^{+} T cell accumulation in tumor microenvironments.

Importantly, however, CD8^{+} T cells in tDLNs (Fig. S1, A and B) and spleens (Fig. 1, F and G) exhibited a more activated phenotype with elevated PD-1 and 1B11 in hematopoietic but not nonhematopoietic chimeras, indicating that some of the intratumoral effect observed in hematopoietic chimeras may result from recruitment of activated systemic populations rather
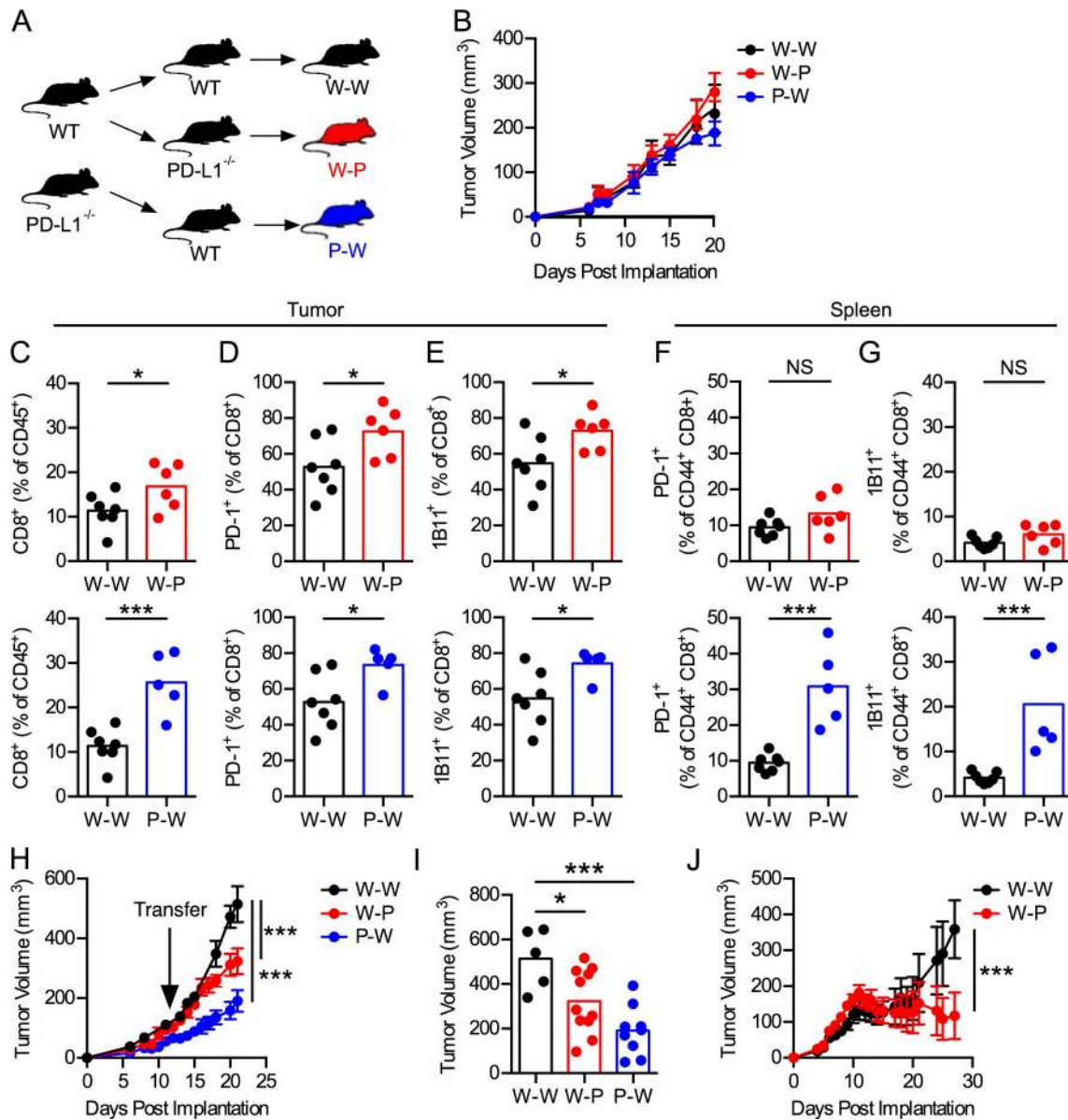
Figure 1. Nonhematopoietic expression of PD-L1 in peripheral tumors limits local cytotoxic T cell function. (A) Lethally irradiated WT or PD-L1$^{-/-}$ mice were reconstituted with WT or PD-L1$^{-/-}$ bone marrow generating WT into WT (W-W; black, controls), WT into PD-L1$^{-/-}$ (W-P; red, nonhematopoietic PD-L1$^{-/-}$), and PD-L1$^{-/-}$ into WT (P-W; blue, hematopoietic PD-L1$^{-/-}$) chimeric mice. **(B)** B16F10.OVA tumor growth in PD-L1$^{-/-}$ bone marrow chimeric mice. Average tumor volume ± SEM, $n > 8$. **(C–G)** W-P or P-W PD-L1$^{-/-}$ chimeras compared with W-W controls. **(C)** Intratumoral CD8$^+$ T cells (%CD45). **(D and E)** PD-1 (D) and 1B11 (E) expression by intratumoral CD8$^+$ T cells. **(F and G)** PD-1 (F) and 1B11 (G) expression by CD8$^+$ T cells in spleens. **(H and I)** In vivo generated effector OT-I TCR-tg CD8$^+$ T cells were transferred into B16F10.OVA tumor–bearing PD-L1 chimeric mice. Tumor growth (H) and final volume (I) of PD-L1$^{-/-}$ chimeric mice. Average tumor volume ± SEM, $n ≥ 5$. **(J)** YUMMER1.7 tumor growth in W-W and W-P PD-L1$^{-/-}$ chimeric mice. Average tumor volume ± SEM, $n = 5$. Each point represents one mouse; bars indicate the mean. One-way ANOVA corrected for multiple comparisons (C–I). One-way ANOVA corrected for multiple comparisons (B, H, and I) or Student's t test (J) performed on average slope and variance of individual tumor growth curves. *, $P < 0.05$; ***, $P < 0.001$.

than release of intratumoral immune suppression. Consistent with these data and a role for hematopoietic PD-L1 in priming (Mueller et al., 2010), CD103$^+$-migratory and CD8α$^+$-resident cross-presenting DCs expressed higher levels of PD-L1 in tDLNs as compared with contralateral, nondraining controls (Fig. S1 C), while no change was observed in constitutive expression by nonhematopoietic LN stromal cells (Fig. S1 D). Thus, to specifically determine the relative contribution of nonhematopoietic and hematopoietic PD-L1 within tumor microenvironments, independent of expanded systemic pools, we transferred ex

vivo–activated (CD44$^+$PD-1$^+$), effector OT-I TCR-Tg CD8$^+$ T cells, whose TCR is MHC class I–restricted to the immunodominant peptide (H2K^b-OVA$_{257–264}$) of OVA, into tumor-bearing chimeras. Increased B16F10.OVA tumor control was observed following adoptive transfer in both chimeras (Fig. 1, H and I), indicating that both hematopoietic and nonhematopoietic PD-L1 limit T cell–mediated tumor control locally.

Given the poor responsiveness of the B16F10 model to single agent PD-L1 therapy, we sought to confirm the role of nonhematopoietic cells in a PD-L1–sensitive murine melanoma model.

YUMM1.7 cells were generated from genetically engineered murine melanomas ($Braf^{V600E};Pten^{-/-};Cdkn2a^{-/-}$) and subsequently treated with three rounds of ultraviolet B radiation to generate YUMMER1.7 cells that exhibit increased somatic mutation burden, sensitivity to single agent immune checkpoint blockade (Meeth et al., 2016; Wang et al., 2017), and regress in PD-L1$^{-/-}$ mice (Fig. S1 E). We implanted YUMMER1.7 cells into WT and nonhematopoietic PD-L1 chimeras to determine whether loss of stromal nonhematopoietic PD-L1 was sufficient to increase tumor control. While YUMMER1.7 tumors grew out in WT-into-WT mice, tumors entered stasis 10 d after implantation in mice lacking nonhematopoietic PD-L1 (Fig. 1 J). Interestingly, since tumors regress in full PD-L1$^{-/-}$ mice (Fig. S1 E), these data are consistent with the hypothesis of synergistic or at least additive effects of hematopoietic and nonhematopoietic PD-L1 in mediating intratumoral T cell exhaustion. As such, in addition to the known role for hematopoietic PD-L1 (Lin et al., 2018; Tang et al., 2018), PD-L1 expression by nonhematopoietic stromal cells contributes to functional suppression of CD8$^+$ T cell accumulation within tumor microenvironments and subsequent tumor control. Furthermore, these data collectively indicate that the functional relevance of nonhematopoietic PD-L1 expression is revealed in the presence of potent, anti-tumor immunity.

LECs and blood endothelial cells (BECs) express PD-L1 in primary murine melanomas and inflamed skin

Given the functional significance of the nonhematopoietic stroma in PD-L1–mediated T cell suppression, we investigated nonhematopoietic PD-L1 expression in various tumor microenvironments. We generated single-cell suspensions from naive skin, B16F10, MC38, YUMM1.7, and YUMMER1.7 tumors and identified CD45$^-$CD31$^+$ tumor-associated LECs (gp38$^+$), BECs (gp38$^-$), and a CD45$^-$CD31$^-$gp38$^+$ stromal population by flow cytometry (Fig. 2 A). Tumor-associated LECs (Fig. 2 B) and BECs (Fig. 2 C) were the highest PD-L1 expressers across tumor models, while gp38$^+$ stromal cells (Fig. 2 D) were largely negative, with the exception of YUMMER1.7 tumors. Interestingly, BECs constitutively expressed PD-L1 in skin, while LEC expression was dependent on tumor context and demonstrated variable expression as a function of their local microenvironment (Fig. 2, B and C). Notably, the highest expression for all cell types was observed in PD-L1–sensitive YUMMER1.7 tumors. We next asked whether PD-L1 expression by LECs was unique to tumors or rather a tissue-based response to local inflammation. Using three different models of cutaneous inflammation, cutaneous infection with Vaccinia virus (VacV; scarification), delayed-type hypersensitivity (DTH; DNFB sensitization), and imiquimod-induced psoriasis, we evaluated LEC PD-L1 expression at sites local and distal to inflammatory challenge. In all models, inflammation enhanced expression of PD-L1 by LECs in affected (Fig. 2 E) but not contralateral (Fig. S2 A) skin as compared with naive, while BECs up-regulated PD-L1 at both sites of challenge and in contralateral, uninflamed skin (Fig. S2, B and C). Thus, while PD-L1 was expressed by BECs under all conditions systemically, LECs demonstrated the highest specificity to local microenvironments and exhibit significantly different levels of PD-L1 expression in checkpoint-sensitive and -insensitive tumors.

Dermal LEC PD-L1 is induced by interstitial, antigen-specific CD8$^+$ T cell immunity

Given the observation that LEC PD-L1 expression was tuned in tumor microenvironments correlating with increasing CD8$^+$ T cell infiltration (Fig. S2 D), we hypothesized that LECs may be directly responsive to infiltrating antigen-specific CD8$^+$ T cells. Due to the robust induction of PD-L1 on LECs in VacV-infected skin 7 d after infection (Fig. 2 E), we used this model for kinetic analysis of EC PD-L1. Flow cytometric analysis of dermal endothelial populations in infected ears at days 0, 3, 7, and 10 after infection revealed peak LEC (100-fold) and BEC (2.5-fold) PD-L1 expression 7 d after infection (Fig. 3 A), concomitant with dermal infiltration of antiviral CD8$^+$ T cells (Hickman et al., 2013; Loo et al., 2017). Depletion of both CD4$^+$ and CD8$^+$ T cells during the first 7 d of infection significantly reduced, but did not eliminate PD-L1 expression by LECs (Fig. 3 B), indicating that T cells are sufficient, but perhaps not necessary to induce LEC PD-L1 expression. This LEC adaptation to infiltrating immunity is reminiscent of mechanisms of adaptive immune resistance described in tumors (Ribas, 2015), therefore we hypothesized that boosted T cell infiltration into tumor microenvironments with low PD-L1 expression would switch on analogous programs of LEC-mediated immune resistance.

To boost a tumor-specific CD8$^+$ T cell response and directly interrogate its effect on LECs, we used a vaccination strategy (attenuated *Listeria monocytogenes*; LM) that induced either nonspecific (LM) or specific (LM-OVA) CD8$^+$ T cell immunity against the model tumor antigen, OVA. As expected, vaccination with LM-OVA slowed B16F10.OVA tumor growth compared with LM-infected or uninfected mice (Fig. 3 C) and boosted the number of total tumor-infiltrating (Fig. S2 E) and H2-K^b–restricted, OVA$_{257-264}$(SIINFEKL)-specific CD8$^+$ T cells (Fig. 3 D). Specific up-regulation of PD-L1 by LECs in tumor microenvironments (Fig. 3 E), and not contralateral skin (Fig. S2 F), and when using LM expressing OVA, and not without, is consistent with a requirement for local antigen recognition. It is likely that antigen recognition is both required for the continued accumulation of these antigen-specific cells at the tumor site and elevated IFNγ. To further test this hypothesis, we adoptively transferred in vitro–activated effector OT-I TCR-Tg CD8$^+$ T cells into tumor-bearing mice. Analysis of tumor-associated LECs 4 d later revealed elevated expression of PD-L1 with transfer relative to steady-state tumors (Fig. 3 F), indicating local antigen-recognition by CD8$^+$ T cells was sufficient to activate regional LECs.

Accumulation of antigen-specific T cells and local TCR activation boosts IFNγ concentrations in tumors (Fig. S2 G), which activates PD-L1 expression through the JAK/STAT pathway (Garcia-Diaz et al., 2017). Neutralization of IFNγ either during the first 7 d of viral infection (Fig. 3 G) or 2 wk of tumor growth (Fig. 3 H) resulted in reduced levels of LEC PD-L1. To investigate whether effector T cells directly activate LECs and induce PD-L1 expression via secretion of IFNγ, naive or in vitro–activated CD8$^+$ T cells were cultured overnight with murine immortalized LECs (iLECs) in the presence or absence of a semipermeable transwell membrane and IFNγ-blocking antibody. In vitro–activated but not naive CD8$^+$ T cells induced PD-L1 expression on LECs dependent on IFNγ and independent of direct cell–cell contact (Fig. 3 I).

Lane et al.
Lymphatic vessels inhibit melanoma immunity

Journal of Experimental Medicine
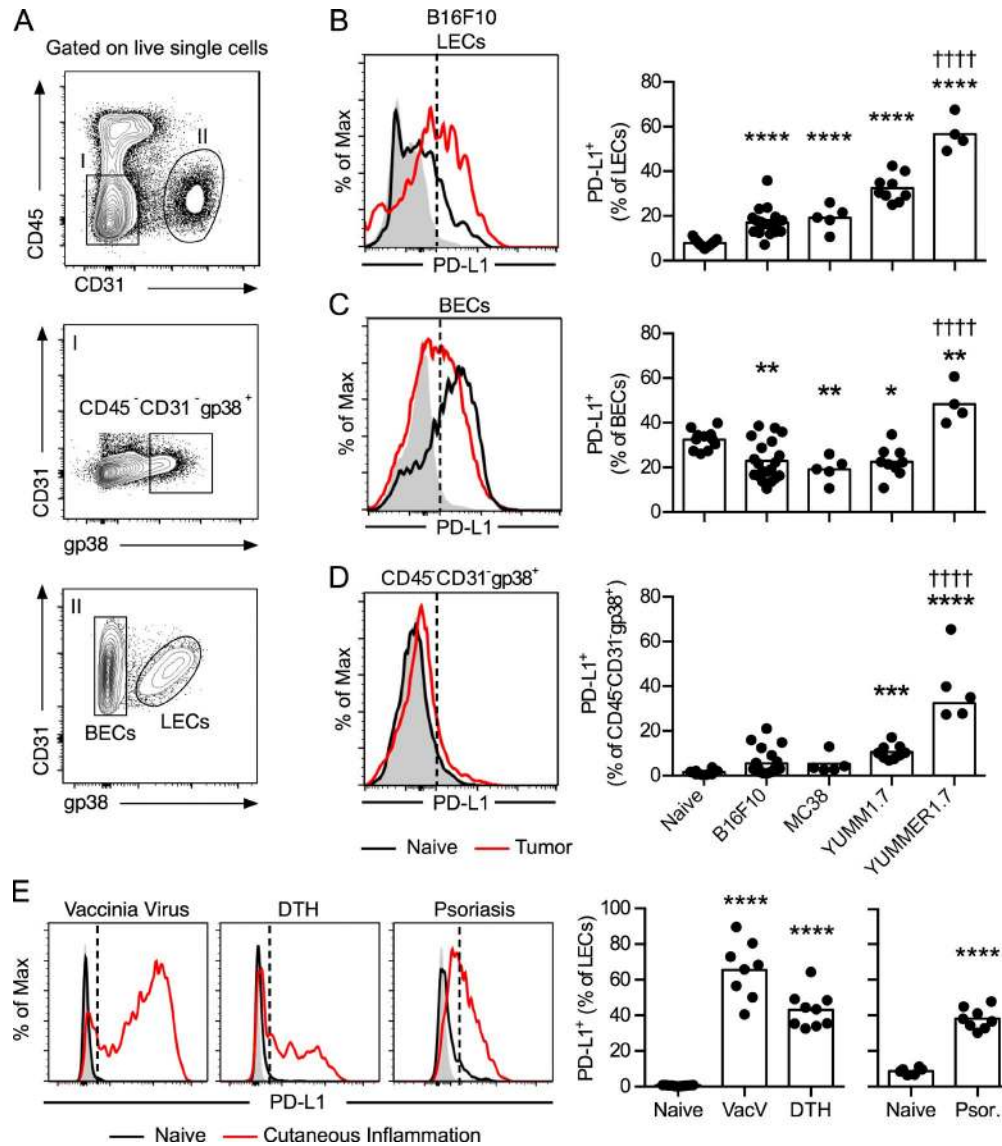https://doi.org/10.1084/jem.20180654

3060

Figure 2. Cutaneous LECs express PD-L1 in inflamed and malignant skin. (A) Gating scheme for LECs (CD45⁻CD31⁺gp38⁺), BECs (CD45⁻CD31⁺gp38⁻), and stromal cells (CD45⁻CD31⁻gp38⁺) from tumors. **(B–D)** Representative histogram (B16F10; left) and quantification (right) of PD-L1 expression by LECs (B), BECs (C), and stromal cells (D) in naive skin, B16F10 melanoma, MC38 colorectal adenocarcinoma, YUMM1.7, and YUMMER1.7 melanoma tumors implanted in the skin of mice. **(E)** Representative histograms (left) and quantification (right) of PD-L1 expression by cutaneous LECs in inflamed skin challenged with VacV, DTH, or imiquimod-induced psoriasis (Psor.) compared with skin of naive mouse (ear or back skin). Each point represents one mouse; bars indicate the mean. Gray histogram represents isotype staining control; dotted line indicates positive gate. One-way ANOVA corrected for multiple comparisons. *, P < 0.05; **, P < 0.01; ***, P < 0.001; ****, P < 0.0001 (compared with naive skin); ††††, P < 0.0001 (compared with B16F10).

Furthermore, IFNγ was sufficient to induce PD-L1 expression in ex vivo murine LECs in a STAT1- and IFNγR-dependent manner (Fig. 3 J) and also in primary human LECs (Fig. 3 K). Consequently, LECs are sensitive to cytotoxic immunity and express PD-L1 in response to IFNγ and local antigen recognition by infiltrating T cells.

IFNγ signaling in lymphatic vessels limits cutaneous anti-viral immunity

We hypothesized that the IFNγ-responsiveness of cutaneous lymphatic vessels might represent a tissue-resident mechanism of immune control that functions to balance protective immunity with immunopathology such that the accumulation of cytotoxic

T cells switches on compensatory mechanisms of immune resolution. To disrupt this crosstalk, we generated mice whose LECs were insensitive to IFNγ by crossing *IFNγR^{f/f}* mice with mice expressing Cre recombinase under control of the lymphatic-specific, lymphatic vessel endothelial hyaluronan receptor 1 (LYVE1) promoter (IFNγR^{ΔLYVE1}). At steady-state, we found no gross change in cutaneous lymphatic vessel structure and density (Fig. S3, A and B), and LN LECs harvested from IFNγR^{ΔLYVE1} mice failed to phosphorylate STAT1 (Fig. S3 C) following IFNγ stimulation, demonstrating the efficiency of the Cre. Macrophages and DCs, as well as other LN stromal cells, including BECs and fibroblastic reticular cells (FRCs), maintained their ability to phosphorylate STAT1 following IFNγ stimulation (Fig. S3 D), indicating specificity of
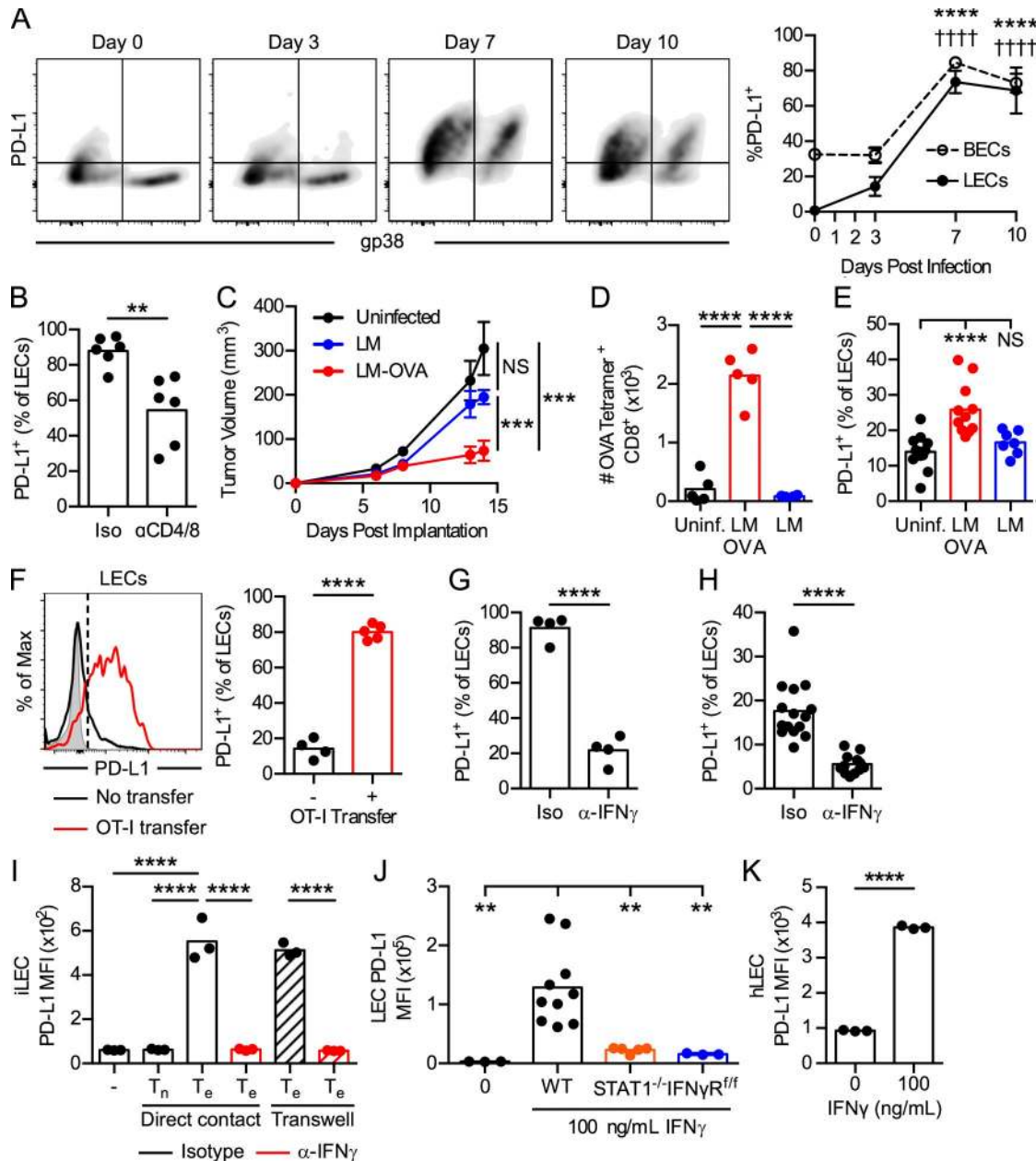
Figure 3. **T cells induce IFNγ-dependent PD-L1 expression in cutaneous LECs. (A)** Representative flow plots (left, gated on CD31$^+$CD45$^-$) and quantification (right) of PD-L1 expression by LECs (CD45$^-$CD31$^+$gp38$^+$) and BECs (CD45$^-$CD31$^+$gp38$^-$) in skin following VacV infection. Mean ± SEM, $n \geq 3$. **(B)** PD-L1 expression by cutaneous LECs 7 d after VacV infection in mice treated with αCD4-/8-depleting antibodies or isotype control. **(C–E)** B16F10.OVA tumor–bearing mice were vaccinated with attenuated (ActA-deficient) LM, expressing OVA (LM-OVA) or not (LM), day 4 after tumor implantation. Iso, isotype. **(C)** B16F10.OVA growth curves. **(D)** Number of H2-K^b–restricted, OVA$_{257-264}$(SIINFEKL)-specific CD8$^+$ T cells in tumors. **(E)** PD-L1 expression by tumor-associated LECs. Uninf., uninfected. **(F)** Representative histograms (left) and quantification (right) of PD-L1 expression by tumor-associated LECs in B16F10-OVA tumor–bearing mice receiving, or not, in vitro–activated OT-I TCR-Tg CD8$^+$ T cells adoptively transferred 10 d after implantation. **(G and H)** PD-L1 expression by cutaneous LECs on day 7 after VacV infection and B16F10 tumor–associated LECs in mice receiving IFNγ-neutralizing antibody or isotype control. **(I)** PD-L1 expression by iLECs following culture with naive (T$_n$) or in vitro–activated, effector CD8$^+$ T cells (T$_e$), treated with αIFNγ or isotype control and separated by semipermeable transwell membranes. Representative of three independent experiments. **(J)** PD-L1 expression by ex vivo–harvested LECs from WT, STAT1$^{-/-}$, or IFNγR$^{\Delta LYVE1}$ mice (IFNγR$^{f/f}$) following 100-ng/ml IFNγ stimulation. **(K)** PD-L1 expression by primary human dermal LECs following IFNγ stimulation. Shaded histogram represents isotype staining control; dotted line indicates positive gate. Each point represents one mouse; bars indicate mean. Student's t test (B, F, G, H, and K) and one-way ANOVA corrected for multiple comparisons (A, D, E, I, and J). One-way ANOVA corrected for multiple comparisons performed on average slope and variance of individual tumor growth curves (C). **, $P < 0.01$; ****, $P < 0.0001$. **** (BECs) and †††† (LECs), $P < 0.0001$ relative to time 0 (A).

the Cre. Importantly, constitutive PD-L1 expression by LN LECs remained unchanged (Fig. S3 E). Interestingly, though previous work indicated that IFNγ was required to limit nodal lymphangiogenesis, we found no gross differences in LN LYVE1$^+$ lymphatic structures at steady-state (Fig. S4, A and B) or when draining implanted melanomas (Fig. S4 C) or VacV-infected skin (Fig. S4 D).

We therefore used this model to ask whether loss of IFNγ sensitivity by peripheral lymphatic vessels (IFNγR$^{\Delta LYVE1}$) impacted

pathology associated with infection and accumulation of anti-viral immunity. Importantly, LEC IFNγR was required for in vivo expression of PD-L1 7 d after infection (Fig. 4 A), while no change was observed in expression by BECs or CD45⁺ leukocytes (Fig. S5, A and B). Loss of IFNγR resulted in a reduction of LYVE1⁺ but not podoplanin⁺ structures in infected skin (Fig. 4, B–D). As LYVE1 can be variably expressed on lymphatic vessels and internalized in regions of active inflammation, these data seem to indicate regional differences in lymphatic vessel activation rather than changes in overall density.

Notably, 7 and 10 d after infection, we observed elevated pathology (Fig. 4 E) in infected ears of IFNγR$^{\Delta LYVE1}$ mice as determined by overall ear thickness (Fig. 4 F) and significant increases in both epidermal (Fig. 4 G) and dermal thickness (Fig. 4 H). Total numbers of CD45⁺ leukocytes in infected ears were significantly elevated 7 d after infection (Fig. 4 I), while the accumulation of CD45⁺ leukocytes in skin as determined by immunohistochemistry (IHC) only trended up at day 10 (Fig. 4 J). We did not observe increased F4/80⁺ macrophage (Fig. 4 K) or mast cell (Fig. 4 L) accumulation in ears 10 d after infection that might explain these changes, but rather saw significant increases in CD4⁺ and CD8⁺ T cell infiltration at day 7 (Fig. 4, M and N). To determine whether IFNγ signaling on LECs negatively regulated antigen-specific CD8⁺ T cell priming, we evaluated CD8⁺ T cells specific for the immunodominant epitope, H2-K^b–restricted, B8R$_{20-27}$(TSYKFESV) in draining LNs (DLNs). 7 d after infection, the peak of T cell expansion, we observed no difference in priming (Fig. 4 O), consistent with normal expression of PD-L1 in lymphoid organs (Fig. S3 E). Within infected tissue, however, there was a twofold enrichment for B8R$_{20-27}$-specific CD8⁺ T cells in ears of IFNγR$^{\Delta LYVE1}$ mice compared with littermate controls (Fig. 4 P). It is noteworthy that the twofold enrichment in antigen-specific T cells doubles an already impressive number of T cells within a single infected ear from 10 × 10⁴ to 20 × 10⁴. While we did not observe accelerated viral control (Fig. 4 Q), as the existing response is already effective at mediating viral clearance, these data taken collectively indicate that IFNγ-dependent adaptation of LECs to skin-infiltrating cytotoxic T cells and expression of PD-L1 functionally limits T cell accumulation that may dampen the pathological response (as determined by dermal and epidermal thickening) in tissue.

CD8⁺ T cells are correlated with and proximal to the lymphatic vasculature in primary human melanoma

For IFNγ and PD-L1–dependent crosstalk between peritumoral lymphatic vessels and tumor-infiltrating CD8⁺ T cells to be functionally relevant, T cells must be proximal to lymphatic vessels in inflamed tissue microenvironments. Immunofluorescence analysis of CD3ε⁺ T cell infiltrates in VacV-infected skin revealed both perilymphatic and intraluminal T cells in infected skin (data not shown), and our previous work demonstrated colocalization of T cells and lymphatic vessels in murine tumors (Lund et al., 2012). We therefore sought to evaluate the correlation between cytotoxic T cells and lymphatic vessels and their spatial proximity in human primary melanomas. We first used a previously established lymphatic score (LS; based on transcript levels of *VEGFC*, *PDPN*, and *LYVE1*; Lund et al., 2016b) to stratify patients from publicly available cutaneous melanoma gene expression datasets

of the Broad Institute's The Cancer Genome Atlas (TCGA). Across both primary and metastatic cutaneous melanoma samples, LS positively correlated with expression of gene transcripts associated with CTLs either as individual transcripts (Fig. 5 A) or a composite score (Fig. 5 B). Samples stratified as LS^{hi} exhibited a statistically significant increase in this T cell inflammation score (Fig. 5 C), a type II IFN score (Fig. 5 D), and expression of *CD274* (PD-L1; Fig. 5 E) and *IDO1* (Fig. 5 F), as compared with LS^{lo} patients, indicating that patients enriched for high expression of lymphatic-associated genes were also enriched for more T cell inflammation and compensatory mechanisms of immune suppression. Importantly, though we found a correlation between LS and T cell inflammation, the strength of the relationship was not sufficient to allow LS-dependent prediction of inflammation, not surprisingly then indicating that other factors contribute to the inflamed status of primary cutaneous melanoma.

To validate the observation that tumor-associated lymphatic vessels correlate with infiltrating T cells, we performed multiplexed IHC (mIHC; Tsujikawa et al., 2017) using formalin-fixed paraffin-embedded (FFPE) human primary melanoma samples (Table S1). We simultaneously evaluated hematopoietic and nonhematopoietic components of tumor microenvironments (Fig. 5 G) and performed spatial proximity analysis to calculate distance from tumor borders. CD8⁺ T cells (Fig. 5 H) and lymphatic vessels (Fig. 5 I) are restricted to the peritumoral stroma in primary melanoma samples, while blood vessels are evenly distributed between intra- and peritumoral regions (Fig. 5 J). The distance of each CD8⁺ T cell to the nearest blood vessel, lymphatic vessel, and tumor cell revealed proximity of all cellular components within the tumor periphery, with CD8⁺ T cells quantitatively closest to blood vessels (Fig. 5 K) but with a significant population of T cells proximal to lymphatic vessels (Fig. 5 L). Importantly, and consistent with our transcriptional analysis, peritumoral LVD positively correlated with peritumoral CD8⁺ T cell density (Fig. 5 M), establishing a correlation between lymphangiogenic tumor microenvironments and T cell infiltration in human melanoma.

Loss of IFNγ signaling on LECs drives CD8⁺ T cell–dependent tumor control and survival

Mechanisms of immune resolution are often coopted by tumors to mediate their immune escape. The enhanced CTL accumulation in virally infected skin (Fig. 4) and proximity of tumor-infiltrating CD8⁺ T cells and tumor-associated lymphatic vessels (Fig. 5) raised the possibility of lymphatic vessel–dependent T cell suppression in melanoma. While loss of nonhematopoietic PD-L1 was functionally significant in bone marrow chimera experiments (Fig. 1), we next asked whether LEC-specific adaptive immune resistance mediated by IFNγ and PD-L1 was relevant in tumor settings. We first implanted PD-L1–insensitive B16F10 (Kleffel et al., 2015) and YUMM1.7 (Meeth et al., 2016) tumors into IFNγR^{WT} and IFNγR$^{\Delta LYVE1}$ mice. In these models, where PD-L1 blockade is ineffective, there was no change in PD-L1 expressed by tumor-associated LECs in IFNγR$^{\Delta LYVE1}$ mice compared with littermate controls (Fig. 6, A and B), and subsequently tumor growth was unaffected (Fig. 6, C and D). Our bone marrow chimera experiments indicated that the functional significance of
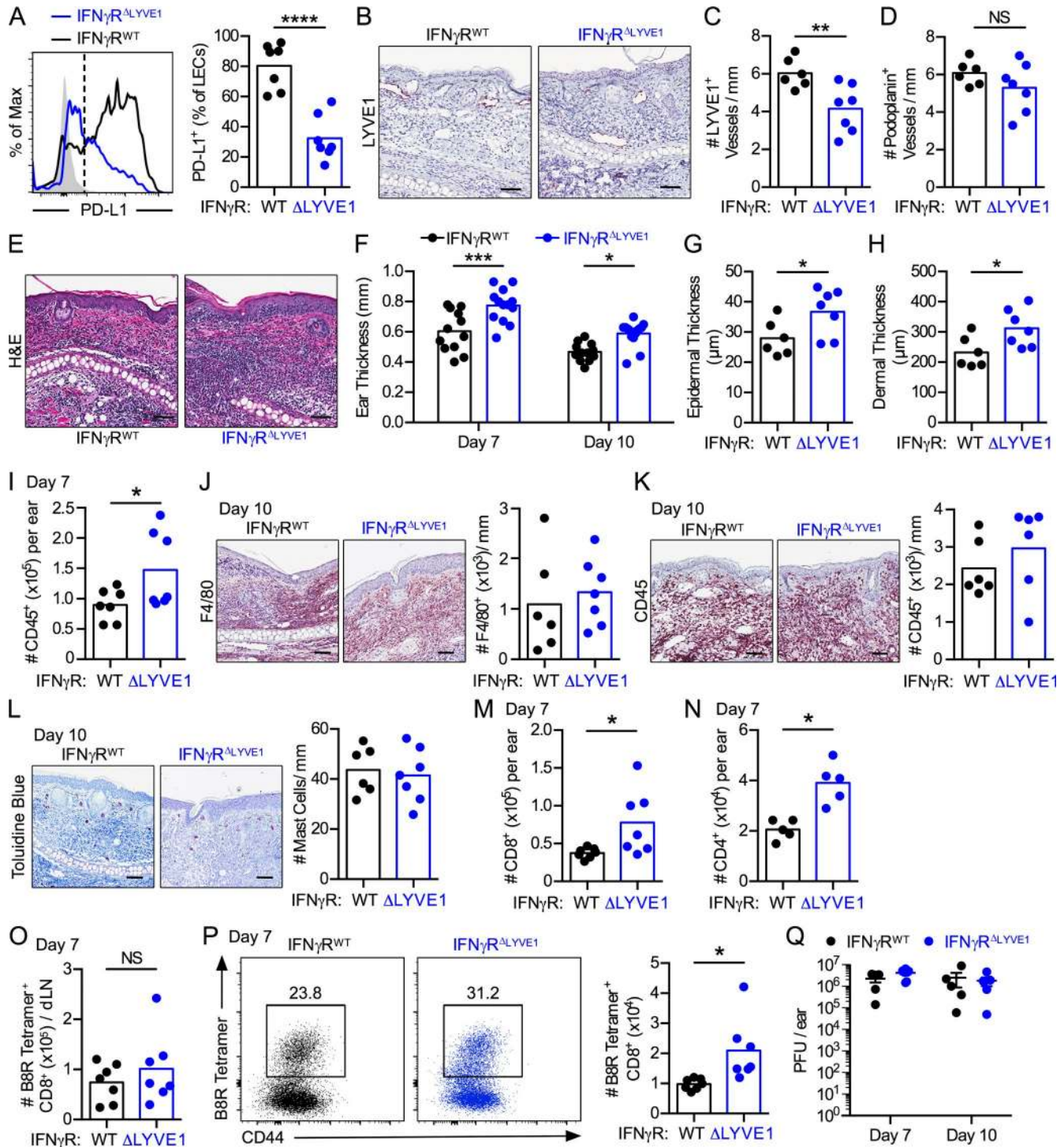
Lane et al.
Lymphatic vessels inhibit melanoma immunity

Journal of Experimental Medicine
https://doi.org/10.1084/jem.20180654

3063

Figure 4. **IFNγ signaling in cutaneous LECs limits anti-viral immunity, but prevents immunopathology. (A)** Representative histogram (left) and quantification (right) of PD-L1 expression by cutaneous LECs 7 d after VacV infection in IFNγR^{ΔLYVE1} mice or littermate controls. **(B–D)** Representative images (B) and quantification of LYVE1$^+$ (C) and podoplanin$^+$ (D) lymphatic vessels in ears of IFNγR^{ΔLYVE1} mice or littermate controls on day 10 after VacV infection. **(E–H)** Representative histology (H&E; E) and quantification of total ear thickness by calipers (F), epidermal thickness (G), and dermal thickness (H) on day 10 after VacV infection in IFNγR^{ΔLYVE1} mice or littermate controls. **(I)** Number of total CD45$^+$ leukocytes in ears of IFNγR^{ΔLYVE1} mice or littermate controls on day 7 after infection. **(J–L)** Representative IHC images and quantification of CD45$^+$ leukocytes (J), F4/80$^+$ macrophages (K), and mast cells (toluidine blue; L) in ears of IFNγR^{ΔLYVE1} mice or littermate controls on day 10 after VacV infection. **(K)** Representative IHC images (left) and quantification (right) of CD45$^+$ cells in ears on day 10 after VacV infection in IFNγR^{ΔLYVE1} mice or littermate controls. **(L–N)** Quantification of total CD8$^+$ T cells (M) and CD4$^+$ T cells (N) in infected skin on day 7 after VacV infection of IFNγR^{ΔLYVE1} mice or littermate controls. **(O)** Total number of H2-K^b–restricted B8R-specific CD8$^+$ T cells in DLNs 7 d after VacV infection. **(P)** Representative plots (gated on CD45$^+$CD8$^+$; left) and quantification (right) of virus-specific H2-K^b–restricted B8R-specific CD8$^+$ T cells in ears of

Lane et al.
Lymphatic vessels inhibit melanoma immunity

Journal of Experimental Medicine
https://doi.org/10.1084/jem.20180654

3064

LEC/T cell crosstalk might be revealed in the setting of more robust preexisting anti-tumor immunity, similar to PD-L1 blockade. Therefore, we looked at the response to LM-OVA vaccination in IFNγR^WT and IFNγR^ΔLYVE1 B16F10-bearing mice. Importantly, LM-OVA primed equivalent systemic OVA-specific responses in both mice (Fig. 6 E); however, LECs failed to activate and up-regulate PD-L1 in IFNγR^ΔLYVE1 mice (Fig. 6 F), while PD-L1 expression on leukocytes and BECs was unchanged (Fig. S5, C and D). Coincident with a failure to up-regulate PD-L1 expression on tumor-associated LECs, we observed improved tumor control with smaller tumors at endpoint (Fig. 6 G) and twofold enrichment of activated, intratumoral tumor-specific CD8^+ T cells (Fig. 6 H). Thus, antigen-specific T cells activate compensatory LEC-specific and IFNγR-dependent mechanisms of local immune control.

While these data demonstrate that, following a therapeutic boost in anti-tumor immunity, intratumoral T cell activity is limited by IFNγ signaling on lymphatic vessels, we were interested in determining whether lymphatic vessel–dependent T cell control might be functional in the absence of vaccination. We therefore implanted the immune checkpoint sensitive YUMMER1.7 cells into IFNγR^WT and IFNγR^ΔLYVE1 mice. Tumor-associated LECs extracted from YUMMER1.7 tumors in IFNγR^ΔLYVE1 mice failed to up-regulate PD-L1 (Fig. 6 I), with no observed change in either lymphatic or blood vessel density (Fig. 6, J–L). Analysis of YUMMER1.7 growth in IFNγR^WT and IFNγR^ΔLYVE1 mice revealed significant tumor control initiated 10 d after implantation, consistent with an adaptive immune response, leading to extended overall survival dependent on CD8^+ T cells (Fig. 6, M and N). We confirmed lymphatic vessel specificity of our result using an inducible *Prox1:Cre^T2* (IFNγR^ΔiProx1). Ex vivo functional analysis confirmed the specificity and efficiency of the *Prox1*-inducible *Cre* (Fig. S3, F–I). Consistent with our results in IFNγR^ΔLYVE1, YUMMER1.7 tumors implanted into IFNγR^ΔiProx1 were controlled relative to Cre-negative mice, again initiating 10 d after implantation, leading to significantly improved overall survival (Fig. 6, O and P). Thus, using two independent systems, we demonstrate that disruption of IFNγ signaling on tumor-associated lymphatic vessels relieves local immune suppression driving persistent and durable tumor-specific CD8^+ T cell responses with similar kinetics to that observed in nonhematopoietic PD-L1 chimeras (Fig. 1 J). These data support the hypothesis that the tumor-associated lymphatic vasculature induces IFNγ-dependent adaptive immune resistance with direct consequences for local, cytotoxic immunity in vivo. Collectively with our results in viral infection, we suggest that IFNγ-mediated activation of the lymphatic endothelium is a tissue-resident protective response limiting tissue damage that is coopted in tumor microenvironments for immune escape.

Discussion

Tissues balance immune activation and immune suppression to mediate rapid response to pathogenic challenge while simultaneously preventing immunopathology and autoimmunity. At environmental barriers, such as skin, the balance between protection and tolerance is even more critical (Cannon et al., 1988), and tumors that arise coopt mechanisms of tolerance to mediate their immune escape. The tissue-specific mechanisms that mediate the balance between immunity and tolerance, and specifically the relative contribution of circulating leukocytes and resident stromal cells, remains an open question.

While hematopoietic cells use multiple mechanisms to suppress cytotoxic T cell accumulation and function in tumor microenvironments, this report demonstrates that nonhematopoietic LECs also regulate immune microenvironments in melanoma. While lymphatic vessel transport is required for de novo priming and expansion of antigen-specific immunity (Lund et al., 2016b; Loo et al., 2017), we show that lymphatic vessel adaptation to infiltrating cytotoxic CD8^+ T cells induces compensatory, suppressive mechanisms that limit local effector function. We find that endothelial adaptation is mediated by IFNγ and part of a broader skin-intrinsic program activated across cutaneous pathologies, including acute viral infection, psoriasis, and DTH. IFNγ sensing by cutaneous LECs activates PD-L1 expression, which we demonstrate is functional within nonhematopoietic stromal cells in tumors. Importantly, LEC-specific loss of IFNγR, and therefore inhibition of the ability for lymphatic vessels to adapt to CTLs, results in elevated pathology following cutaneous infection and improved tumor control.

Interestingly, T cells and IFNγ are implicated as negative regulators of LN lymphatic sinus development and inflammation-induced LN lymphangiogenesis (Kataru et al., 2011). Our analyses did not reveal significant changes in gross LVD in either LNs or skin in IFNγR^ΔLYVE1 mice, perhaps indicating that T cell–mediated control of lymphangiogenesis is IFNγ-independent. Interestingly, recent work demonstrates that type I rather than type II IFNs regulate contraction of LN lymphangiogenesis and that type I IFN–induced PD-L1 expression in a subset of LN LECs protects these cells from apoptosis (Lucas et al., 2018). The molecular mechanisms downstream of type I IFN and PD-L1 that mediate LEC survival, however, remain unclear. Notably, loss of IFNγR on LECs did not affect constitutive PD-L1 expression in LNs, and as such, we saw no changes in LN lymphatic structures at steady-state or during active inflammation and no changes in peripheral T cell priming. Similarly, in skin, we saw no difference in LVD; however, it is important to note that lymphatic vessels in highly inflamed regions of infected IFNγR^ΔLYVE1 skin, but not adjacent normal, were negative for LYVE1. Inflamed lymphatic vessels were identified instead by their expression of podoplanin, thus leading to a reduction in LYVE1^+ but not podoplanin^+ structures in IFNγR^ΔLYVE1-infected skin. Inflammation induces internalization of LYVE1 (Johnson et al., 2007), and thus, loss of expression on LYVE1^+ structures may be a readout of local inflammation. Additionally, however, it is possible that loss of LYVE1 on peripheral lymphatic vessels is IFNγR-dependent, and given the role of

---

IFNγR^ΔLYVE1 mice or littermate controls 7 d after VacV infection. **(Q)** Viral titers in IFNγR^ΔLYVE1 mice or littermate controls on day 7 and 10 after VacV infection. Shaded histogram represents isotype staining control; dotted line indicates positive gate. Each point represents one mouse; bars indicate mean. Scale bars, 100 μm. Student's *t* test (A–D and G–P); one-way ANOVA corrected for multiple comparisons (F and Q); *, P < 0.05; **, P < 0.01; ***, P < 0.001; ****, P < 0.0001.
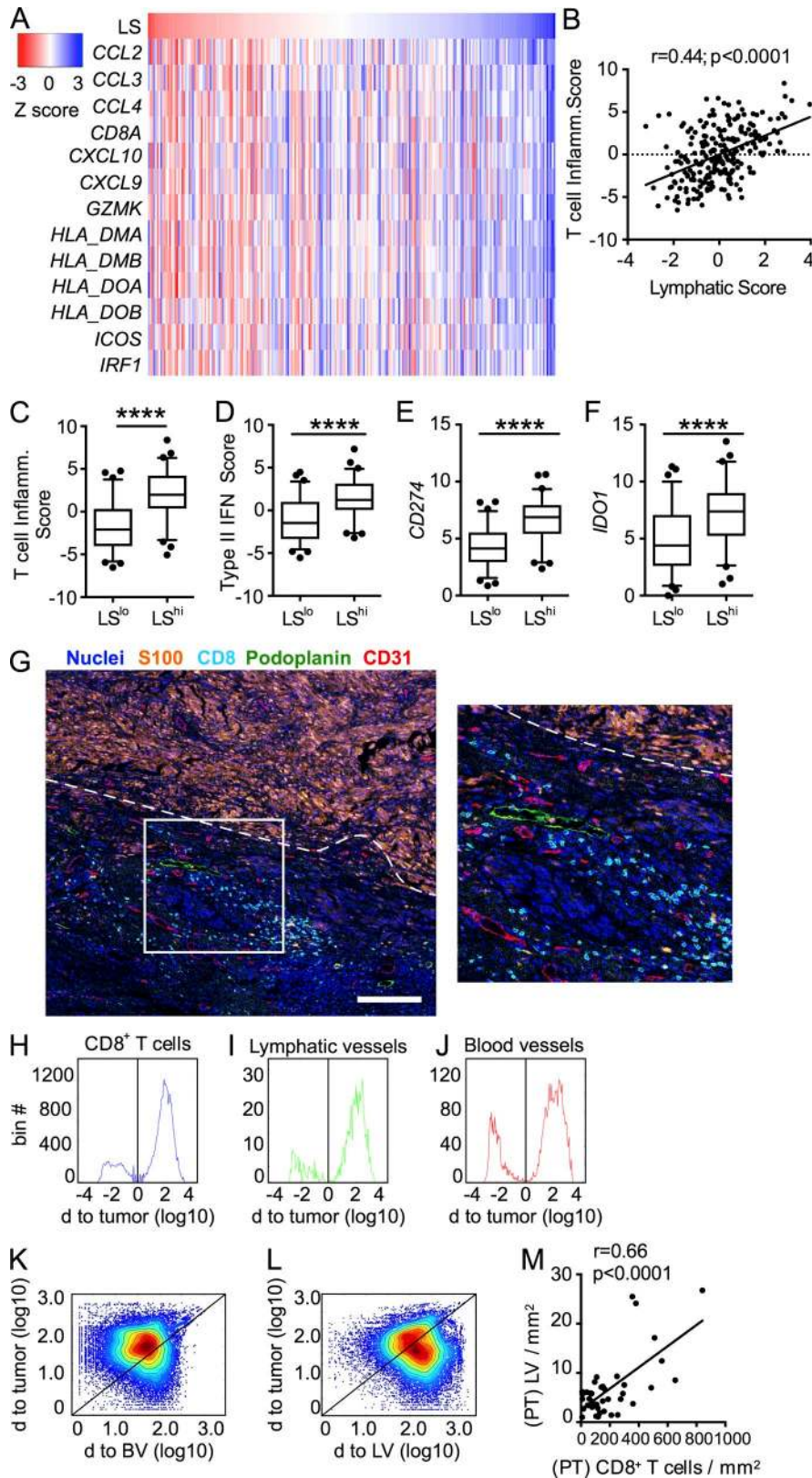
Figure 5. **Tumor-associated lymphatic vessels correlate with and are proximal to T cell infiltrates in human primary melanoma. (A)** Heat map clustering of genes associated with T cell inflammation and LS (*VEGFC*, *PDPN*, and *LYVE1*) across 231 primary and metastatic (nonglabrous and nonlymphoid) patient samples from the Broad Institute's TCGA database. **(B)** Correlation between lymphatic and T cell inflammation scores. Pearson's correlation coefficient (r). **(C–F)** Stratification of LS into high (LS^{hi}; n = 68) and low (LS^{lo}; n = 71) cohorts stratifies T cell inflammation score (C), type II IFN score (D), *CD274* expression (E), and *IDO* expression (F) melanoma samples. Box plots; whiskers indicate 5th–95th percentile with outliers. Student's *t* test; ****, P < 0.0001. **(G)** Digital overlay of pseudo-colored single stains from mIHC of FFPE human primary melanomas. Representative image and inset. H&E (nuclei, blue); S100 (orange); CD8 (cyan); D2-40 (podoplanin, green); and CD31 (red). Scale bar, 200 µm. **(H–J)** Distribution of CD8$^+$ T cell (H), D2-40$^+$ lymphatic vessel (I), and CD31$^+$ blood vessel (J) distance from S100$^+$ tumor border. **(K and L)** Scatter plots represent shortest distance from CD8$^+$ cells to S100$^+$ tumor border versus CD31$^+$ vessels (K) and D2-40$^+$ lymphatic vessels (L). **(M)** Correlation between peritumoral (PT) LVD and PT CD8$^+$ T cell density, compiled data across n = 17 samples and 40 regions of interest.

LYVE1 in DC transendothelial migration (Johnson et al., 2017), this may be intriguing to investigate in the future.

IFNγ may be a common mechanism governing tissue homeostasis, immune resolution, and tumor immune evasion. Migratory DCs respond to IFNγ at steady-state and inhibit T cell priming as a mechanism of peripheral tolerance, and tumors recall this homeostatic program to prevent robust anti-tumor immune activity (Nirschl et al., 2017). Our data further demonstrate that IFNγ-mediated crosstalk between the tumor-associated lymphatic vasculature and infiltrating CTLs has a negative impact
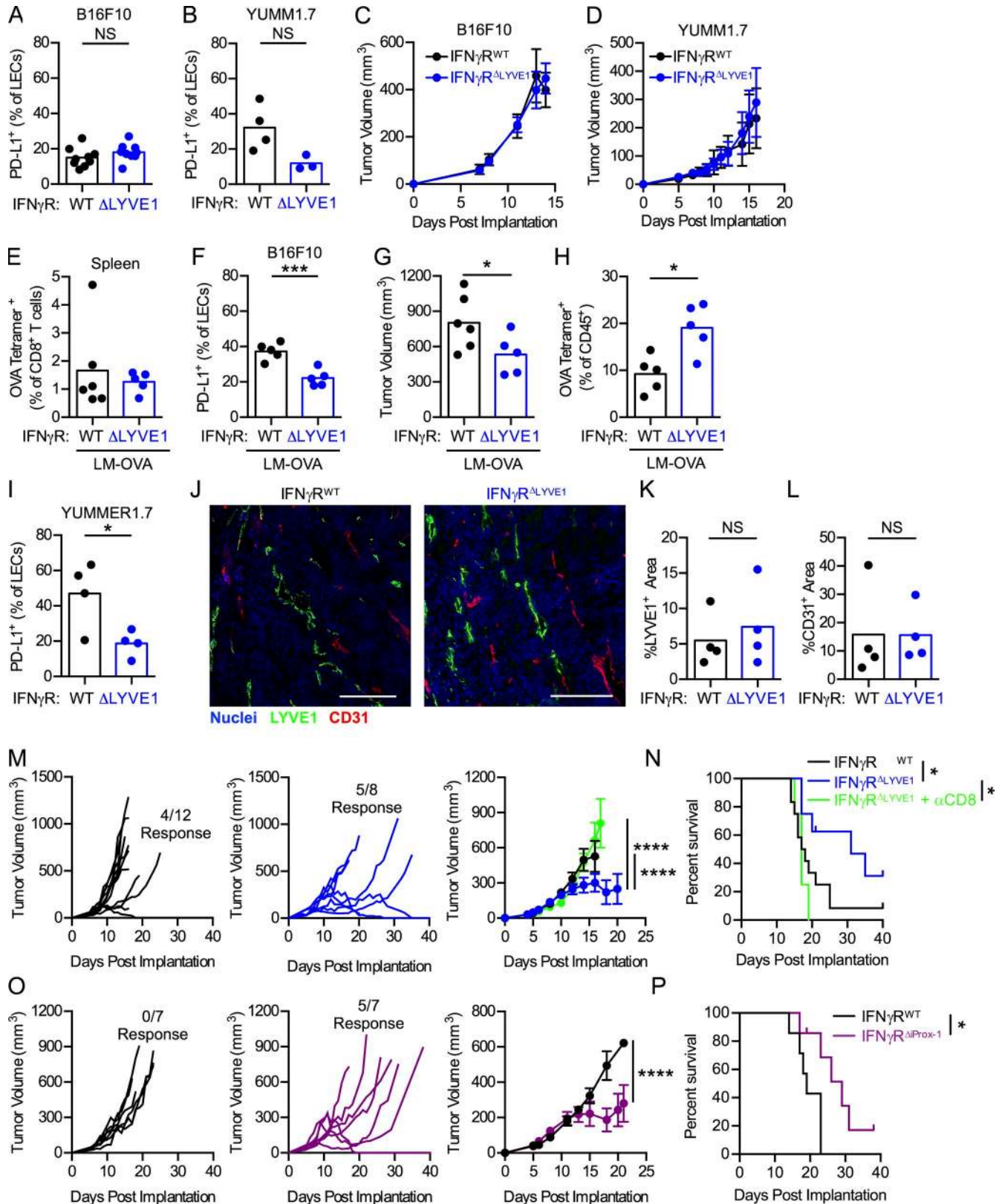
Figure 6. **Disrupting IFNγ-mediated LEC crosstalk with T cells enhances CD8+ T cell–dependent melanoma control. (A and B)** Quantification of tumor-associated LEC PD-L1 expression in B16F10 (A) and YUMM1.7 (B) tumors implanted into IFNγR$^{\Delta LYVE1}$ mice or littermate controls. **(C and D)** B16F10 (C) and YUMM1.7 (D) tumor growth in IFNγR$^{\Delta LYVE1}$ mice or littermate controls. **(E)** H2-K^b–restricted OVA-specific CD8+ T cells in spleens of B16F10.OVA tumor–bearing IFNγR$^{\Delta LYVE1}$ mice or littermate controls vaccinated with LM-OVA. **(F)** PD-L1 expression by LECs in B16F10.OVA tumors of IFNγR$^{\Delta LYVE1}$ mice or littermate controls vaccinated with LM-OVA. **(G)** Final B16F10.OVA tumor volumes IFNγR$^{\Delta LYVE1}$ mice or littermate controls vaccinated with LM-OVA. **(H)** H2-K^b–restricted OVA-specific tumor-infiltrating CD8+ T cells from tumors of mice in G. **(I)** PD-L1 expression by LECs in YUMMER1.7 tumors implanted into IFNγR$^{\Delta LYVE1}$ mice or

Lane et al.
Lymphatic vessels inhibit melanoma immunity

Journal of Experimental Medicine
https://doi.org/10.1084/jem.20180654

3067

on anti-tumor immunity. Thus, while IFNγ is critical for effector function within tumor microenvironments (Ikeda et al., 2002), it may additionally signal to initiate programs of resolution and evasion where multiple cell types, both hematopoietic and non-hematopoietic, contribute. These mechanisms compete with cytotoxic activity in tumors and may partially explain the poor utility of IFNγ treatment in the clinic, where it was found to induce T cell suppression (Creagan et al., 1988; Osanto et al., 1989). Importantly, while T cells are sufficient to activate IFNγ-dependent mechanisms of immune suppression, they are not necessary, and other IFNγ secreting cells, such as natural killer cells, may also contribute.

One component of IFNγ-driven immune evasion in tumors, termed adaptive immune resistance (Ribas, 2015), is the expression of the immune checkpoint PD-L1. Several recent reports specifically demonstrate that loss of PD-L1 by either tumor cells or the host, into which those cells are implanted, results in improved tumor control (Juneja et al., 2017; Lin et al., 2018; Tang et al., 2018), providing strong evidence that PD-L1 expressed by the tumor microenvironment is relevant for therapy. These studies, however, did not interrogate the role of nonhematopoietic, nontumor PD-L1 expression, leaving this question open. Similar to our data, the functional significance of loss of PD-L1 on one or more cellular components within the tumor microenvironment is highly dependent on the model chosen (Juneja et al., 2017), indicating multiple, overlapping mechanisms that mediate immune escape. That the functional relevance of lymphatic vessel IFNγR was revealed only in immunogenic tumor models (YUMMER1.7) and when T cell–activating therapies (LM and adoptive T cell transfer) were administered to poorly immunogenic tumors (B16F10 and YUMM1.7) supports the model of adaptive immune resistance whereby infiltrating CTLs activate multiple mechanisms of local immune suppression (e.g., IDO, regulatory T cells, etc.) that ultimately feedback and limit their function. Importantly, growth of a variety of melanoma cell lines in mice whose lymphatic vessels lack IFNγR directly mirrors their sensitivity to PD-L1 blockade in vivo. Furthermore, while these adaptive mechanisms of suppression are activated in the presence of potent immunity, alternative mechanisms of tumor suppression are dominant in progressing, poorly immunogenic tumors. Notably, myeloid-targeted therapy effectively mobilized anti-tumor CTLs in checkpoint-insensitive YUMM1.7 tumors (Pan et al., 2017; Hoves et al., 2018; Perry et al., 2018).

Our data importantly extend previously reported roles for nonhematopoietic PD-L1 in infection (Mueller et al., 2010; Frebel et al., 2012) and sterile inflammation (Scandiuzzi et al., 2014) to tumor microenvironments. During chronic lymphocytic choriomeningitis (LCMV) infection, nonhematopoietic PD-L1 delays viral clearance, but prevents overt immunopathology (Mueller et al., 2010), where loss of PD-L1 on infected endothelium leads to barrier breakdown and fatal circulatory failure (Frebel et al., 2012). LCMV importantly infects vascular endothelium, and as such, PD-L1 protects endothelial cells from cytotoxic killing. Here we demonstrate that loss of IFNγR and thus PD-L1 expression on LECs during acute viral infection increased VacV-specific CD8+ T cell accumulation in skin, leading to enhanced local pathology, though viral clearance was unaffected. Importantly, LECs are not directly infected in this model (Loo et al., 2017); however, it is unknown whether antigen-presentation is necessary for the observed PD-L1–dependent T cell control. In tumors, both tumor and myeloid cells express PD-L1 and their simultaneous presentation of antigen may also be required for PD-L1–dependent inhibition of CD8+ T cell effector function (Juneja et al., 2017). While LECs are capable of scavenging and cross-presenting antigen to CD8+ T cells in vitro (Hirosue et al., 2014) and in vivo (Lund et al., 2012) and inhibition of PD-L1 on antigen-pulsed LECs in vitro enhances CD8+ T cell priming (Dieterich et al., 2017), whether tumor-specific antigen presentation is required for effector CD8+ T cell control mediated by LEC PD-L1 in vivo remains unclear.

Alternatively, PD-L1 may function on nonhematopoietic cells to regulate lymphocyte migration across barrier tissues, both endothelial and epithelial. PD-L1 expressed on BECs inhibits transmigration in multiple sclerosis (Pittet et al., 2011), loss of PD-L1 on corneal epithelium results in pathological CD8+ T cell infiltration and chronic dry eye disease (El Annan et al., 2010), and PD-1 on islet-specific CD4+ T cells impairs pancreatic infiltration and diabetes onset in mice (Pauken et al., 2013). Furthermore, normalizing doses of anti-angiogenesis therapy induced PD-L1 expression by tumor-associated blood vessels, leading to a synergistic response with PD-1 blockade and improved CTL infiltration into tumor parenchyma (Schmittnaegel et al., 2017). Whether PD-L1 expressed on endothelial cells specifically regulates T cell transendothelial migration in the absence of simultaneous antigen presentation remains to be carefully studied in vivo.

Herein, we provide two lines of evidence to support in vivo functionality of nonhematopoietic LEC PD-L1. First, we generate bone marrow chimeras that lack PD-L1 expression on hematopoietic and nonhematopoietic cells to demonstrate that nonhematopoietic PD-L1 expression, in addition to expression by hematopoietic cells, influences intratumoral T cell activity. Second, we eliminate induction of PD-L1 expression in a cell-specific manner by preventing LEC response to IFNγ. Using two lymphatic-specific Cre recombinases, we demonstrate that loss of IFNγ sensitivity specifically in lymphatic vessels unleashes CD8+ T cell immunity within tumor microenvironments, leading to persistent tumor control. Furthermore, using the immunogenic melanoma cell line YUMMER1.7, we demonstrate that both loss of nonhematopoietic PD-L1 and loss of lymphatic vessel IFNγR exhibit similar patterns of tumor control, which initiate following T cell accumulation in tumors ~10 d after implantation. It is still

littermate controls. **(J–L)** Representative immunofluorescence images and quantification (K and L) of lymphatic vessels (green, LYVE1; K), blood vessels (red, CD31; L) in YUMMER1.7 tumors implanted into IFNγR^ΔLYVE1 mice or littermate controls. Scale bars, 200 µm. **(M and N)** YUMMER1.7 tumor growth (M) and survival (N) of IFNγR^ΔLYVE1 mice (blue), IFNγR^ΔLYVE1 mice treated with CD8-depleting antibody (green) or littermate controls (black). **(O and P)** YUMMER1.7 tumor growth (O) and survival (P) of IFNγR^ΔiProx1 mice (purple) or littermate controls (black). Each point represents one mouse, bars indicate mean. Student's *t* test (A, B, and E–I). One-way ANOVA corrected for multiple comparisons (M) or Student's *t* test (C, D, and O) performed on average slope and variance of individual tumor growth curves Mantel-Cox test used for comparison of survival (N and P); *, P < 0.05; ***, P < 0.001; ****, P < 0.0001.

Lane et al.
Lymphatic vessels inhibit melanoma immunity

Journal of Experimental Medicine
https://doi.org/10.1084/jem.20180654

3068

possible, however, that a broader program of IFNγ-dependent immune suppressive mechanisms contribute to the observed effects seen following lymphatic vessel-specific IFNγR deletion, and thus, further exploration of the cellular and molecular mechanisms regulated by IFNγ on peripheral lymphatic vessels is warranted.

Importantly, we observed systemic expansion of effector immunity in both PD-L1$^{-/-}$ mice and those treated with antibodies blocking PD-L1. Loss of PD-L1 in the hematopoietic compartment was sufficient for systemic effects indicating that hematopoietic PD-L1 may function to limit T cell priming or expansion in response to tumor antigen presentation in DLNs, as is also seen in LCMV Clone 13 infection (Mueller et al., 2010). Consistent with the hypothesis that new lymphocyte recruitment contributes to PD-L1–based therapies, administration of the small molecule FTY720, to prevent LN egress, inhibits α-PD-L1 therapy in tumor models (Tang et al., 2018). We observe elevated PD-L1 expression on migratory, cross-presenting CD103$^+$ DCs required for antigen-specific T cell priming in LNs draining murine melanoma (Roberts et al., 2016), while nonhematopoietic PD-L1 expression in LN stromal cells (Tewalt et al., 2012) remains unchanged. Thus, our data, together with recently published work, indicate distinct roles and anatomical sites of action for hematopoietic and nonhematopoietic PD-L1 in the host response to tumors.

Finally, our data expand our model of lymphatic vessel contribution to anti-tumor immunity (Lund, 2016). VEGF-C–driven tumor-associated lymphangiogenesis is correlated with increased intratumoral inflammation and immune suppression in progressing tumors (Lund et al., 2012), but also generates tumor microenvironments more amenable to immunotherapeutic intervention (Fankhauser et al., 2017). It is interesting to speculate that the suppressive mechanism elucidated here may explain the improved response to immune checkpoint blockade in lymphangiogenic tumors (Fankhauser et al., 2017). While lymphatic vessels promote the recruitment and accumulation of T cell inflammation in tumor microenvironments, we show that their activation in this context generates negative feedback that, if inhibited, revives peripheral immune responses. As such, lymphatic vessels may be necessary for positive response to immune checkpoint blockade. Furthermore, and consistent with previous work demonstrating that LVD stratifies tumors with elevated tumor-infiltrating lymphocytes (Lund et al., 2016b; Mlecnik et al., 2016; Bordry et al., 2018), we demonstrate that the lymphangiogenic tumor stroma in primary human melanoma accumulates significant CD8$^+$ T cell infiltrates. It is important to note that our samples exhibited a dominant excluded infiltrate phenotype and thus our specific correlation with peritumoral infiltrates. Whether changes in LVD only predict peritumoral rather than intratumoral accumulation remains to be evaluated in larger cohorts. A broader range of T cell involvement in melanoma, however, is captured by TCGA analysis, which indicates correlation between lymphatic-specific genes and T cell inflammation across all tumors, though the geographic distribution of T cells is lost.

Our cumulative work now demonstrates that while the existing lymphatic vasculature is required for de novo T cell priming (Lund et al., 2016b; Loo et al., 2017), the remodeled, inflamed peripheral lymphatic vasculature sequesters and inhibits effector immunity directly in peripheral tissue, leading to tumor progression and contributing to locoregional metastasis (Skobe et al., 2001; Pasquali et al., 2013). Ultimately, though therapies targeting the suppressive tumor microenvironment can rescue anti-tumor immunity, tissues activate multiple compensatory mechanisms to limit effector T cell immunity, driving return to homeostasis and immune escape.

Taken altogether, the lymphatic vasculature, as a part of the nonhematopoietic tumor stroma, is an active barrier to the effector arm of anti-tumor immune responses. The lymphatic vasculature activates programs of adaptive immune resistance following accumulation of interstitial antigen-specific immunity, thus acting as a tissue-resident, immunological switch that balances immune function and damage. We propose that tissues provide a physical scaffold within which immune responses must exert their effector function and therefore are important regulators of local responses. It is interesting to speculate how, as this tissue microenvironment is altered by pathological state, environmental challenge, or age, regional immunity may be similarly altered. Consideration of these tissue-specific effects may provide critical insight into the heterogeneous responses observed across tissue and tumor sites (Reuben et al., 2017) and may provide unique biomarkers of therapeutic response and consequently new local targets for clinical intervention.

Materials and methods

Mice
Specific pathogen–free C57BL/6J and B6 CD45.1 Pep Boy mice were purchased from The Jackson Laboratory. PD-L1$^{-/-}$ were provided by H.O. Vandenbark (Oregon Health and Science University [OHSU], Portland, OR), and Prox1:Cre-ER^{T2} mice were provided by V.H. Engelhard (University of Virginia, Charlottesville, VA) in agreement with T. Makinen (Uppsala University, Uppsala, Sweden). Tg(TcraTcrb)1100Mjb/J (OT-I mice, stock no. 003831), Lyve1 (stock no. 012601), and IFNγR$^{fl/fl}$ (stock no. 025394) mice were purchased from Jackson, and all breeding was maintained at OHSU in specific pathogen–free facilities. All mice were previously backcrossed over 10 generations to the C57BL/6 background. Tyr:Cre-ER (stock no. 012328), Braf^{V600E} (stock no. 017837), and Pten$^{fl/fl}$ (stock no. 006440) mice were purchased from The Jackson Laboratory and crossed in-house to generate Tyr::CreER;Braf$^{CA/+}$;Pten$^{fl/fl}$ (BPC) mice for tumor induction. For all in vivo studies, sex-matched 8–10-wk-old mice were used with at least three to five mice per group. Bone marrow chimeras were sex-matched 16–20-wk-old mice. LNs from STAT1$^{-/-}$ mice were donated by the T.J. Nice laboratory (OHSU, Portland, OR). All animal procedures were approved by and performed in accordance with the Institutional Animal Care and Use Committee at OHSU.

Cell lines
B16F10 (stock no. CRL-6475; ATCC), B16F10.OVA murine melanoma, and MC38 murine adenocarcinoma cells (stock no. CRL-6475; ATCC) were passaged in DMEM (Invitrogen) supplemented with 10% FBS (Atlanta Biologicals) and 1% penicillin-streptomycin (Gibco). Yumm1.1, Yumm1.7 (Meeth et al., 2016), and YUMMER1.7 (Wang et al., 2017) were passaged in 1:1 DMEM: F-12 supplemented with 1% L-glutamine, 1% nonessential amino

Lane et al.
Lymphatic vessels inhibit melanoma immunity

Journal of Experimental Medicine
https://doi.org/10.1084/jem.20180654

3069

acids, 10% FBS, and 1% penicillin-streptomycin. iLECs (Hirosue et al., 2014) passaged in 1:1 low glucose DMEM/F12 (Gibco), supplemented with 20% FBS, 1% penicillin-streptomycin, Bovine endothelial cell growth supplement (10 µg/ml; BD Biosciences), heparin (56 µg/ml; Sigma-Aldrich), and IFNγ (100 ng/ml). Primary human LECs (lonza hmVEC-dLy, CC-2810) were cultured according to the manufacturer's recommendation.

Tumor studies
5×10^5 B16F10.OVA, MC38, YUMM1.7, or YUMMER1.7 tumor cells were implanted intradermal into the flank of mice. Tumor growth was measured daily using digital calipers to measure the long and short axis. Average diameters were used to calculate spherical volume. Tumors were harvested and digested with collagenase I and II (Gibco), collagenase IV (Gibco), or collagenase D (Sigma-Aldrich) for 30–60 min at 37°C. Digests were then passed through a metal screen and 70-µm pore filter. Enrichment for lymphocytes was performed using a Lymphoprep gradient (StemCell Technologies) according to the manufacturer's protocol.

LM infection
ActA-deficient LM was grown in tryptic soy broth (Sigma-Aldrich) supplemented with 50 µg/ml streptomycin (Sigma-Aldrich) at 37°C until OD600 = 0.1 (10^8 CFU/ml). 10^7 CFUs in 200 µl PBS were transferred intravenously into mice.

VacV infection
VacV expressing the recombinant antigen (VacV-GP33) was propagated in BSC-40 cells using standard protocols. Mice were infected cutaneously by 25 pokes with a 29-G needle following administration of 5×10^6 PFUs VacV in 10 µl PBS to the ventral side of the ear pinna (scarification). Virus is propagated using standard protocols. Ear thickness was measured by digital calipers.

Imiquimod-induced psoriasis
Psoriasis was induced using imiquimod, as previously described. Specifically, the back hair of C57BL6 mice was removed using an electric razor. Mice received a daily topical dose of 62.5 mg 5% Imiquimod Cream (Perrigo) or Cetaphil cream, as vehicle control, for 4 d. Mice were sacrificed, and skin was collected on day 5.

DTH
DTH was induced by application of DNFB solution (150 µl 0.5%) in acetone/olive oil (4:1) to shaved backs of mice. 4 d later, right ears were challenged with DNFB solution (20 µl of 0.3%), and left ears were treated with vehicle. Animals were sacrificed 2 d later.

Human melanoma samples
5-µm sections of archived FFPE of stage I and II human primary melanoma resections were obtained from the OHSU Knight Biolibrary and the OHSU Department of Dermatology research repository (Table S1). Acquisition and use of human samples was performed in accordance with the Institutional Review Board at OHSU.

Flow cytometry and antibodies
The following fluorescent dye–conjugated antibodies against surface and intracellular antigens were used: B2-20 (RA3-6B2;

BioLegend), CD103 (2E7; BioLegend), CD106 (429; BioLegend), CD11b (M1/70; BioLegend), CD11c (N418; BioLegend), CD31 (MEC 13.3; BD Biosciences), CD3ε (145-2C11; BioLegend), CD4 (GK1.5; BioLegend), CD43 activation-glycoform (1B11; BioLegend), CD44 (IM7; Tonbo), CD45 (30-F11; BioLegend), CD45.1 (A20; BioLegend), CD45.2 (104; Tonbo), CD8 (53-6.7; Tonbo), CD90.1 (OX-7; BioLegend), F4/80 (BM8; BioLegend), I-A/I-E (M5/114.15.2; BD Biosciences), IFNγ (XMG1.2; Tonbo), PD-1 (29F.1A12), PD-L1 (MIH5; BD Biosceinces), podoplanin (8.1.1; BioLegend), pSTAT1 (612564; BD Biosciences), and TNFa (MP6-XT22; BioLegend). Single-cell suspensions were prepared from tumors by digestion with collagenase D (1 mg/ml; Sigma-Aldrich) and DNase (50 U/ml, for leukocyte extraction; Sigma-Aldrich) or collagenase IV (2200 U/ml; Worthington Biomedical) and DNase (50 U/ml, for endothelial cell extraction; Sigma-Aldrich). Whole-tissue suspensions were then generated by gently forcing the tissue through a wire mesh screen, then filtered through 70-µm pore nylon cell strainers. Leukocytes were enriched using Lymphoprep (StemCell Technologies) as per the manufacturer's instructions. Single-cell suspensions were stained and fixed with 2% paraformaldehyde. All data were acquired with a BD Biosciences Fortessa or LSRII flow cytometer and analyzed using FlowJo Software (TreeStar Inc.). Intracellular cytokine staining was performed as described above and fixed with BD Cytofix/Cytoperm (BD Biosciences). All antibodies were obtained from BD Biosciences, BioLegend, or Tonbo Biosciences unless otherwise specified. H2-K^b–restricted, B8R$_{20-27}$, and Ova.SIINFEKL Tetramers were obtained from the National Institutes of Health tetramer core facility.

IHC and immunofluorescence
Immunofluorescence
LNs were fixed in 1% paraformaldehyde (24 h at 4°C), transferred to 15% sucrose (overnight at 4°C), followed by 30% sucrose (overnight at 4°C), and then indirectly frozen in optimal cutting temperature compound (23-730-571; Thermo Fisher Scientific). 30-µm sections (Cryotome; Thermo Fisher Scientific) were blocked using 1:1 2.5% normal goat serum/2.5% BSA solution, and primaries were added for 2 h at room temperature. Sections were stained with secondary in 1.25% BSA for 1 h at room temperature, followed by incubation with DAPI nuclei stain (Thermo Fisher Scientific) for 5 min at room temperature. Slides were sealed with SlowFade Gold antifade reagent (Invitrogen) and imaged a Zeiss ApoTome.2 fluorescent microscope (Carl Zeiss) and processed using ZEN software (Carl Zeiss). Antibodies were as follows: CD3ε (550277; BD Biosciences), B220 (RA3-6B2; BioLegend), and LYVE1 (103-PA50; Reliatech); and anti-hamster A546 (A21111), anti-rabbit A488 (A21206), and anti-rat A647 (A21472) from Life Technologies.

IHC
Tissues were isolated from mice and fixed in 10% formalin for 24 h at room temperature. Tissues were dehydrated and then embedded in paraffin wax and cut in 7-µm sections. Heated citrate antigen retrieval was performed for 15 min (HK086; BioGenex). Sections were blocked with 2.5% BSA for 1 h at room temperature and then stained for 2 h with primary antibodies in

Lane et al.
Lymphatic vessels inhibit melanoma immunity

Journal of Experimental Medicine
https://doi.org/10.1084/jem.20180654

3070

1.25% BSA at room temperature. Sections were stained with species-matched HRP-conjugated ImmPress polymers (VectorLabs) for 1 h at room temperature and visualized using Bajoran purple (SKU BJP811; BioCare Medical). Sections were imaged on a Leica Aperio Scanscope AT slide scanner and processed using Aperio Imagescope (Leica Biosystems). Antibodies were as follows: CD3ε (550277; BD Biosciences), B220 (RA3-6B2; BioLegend), LYVE1 (103-PA50; Reliatech), F4-80 (CL;A3-1; BioRad), CD45 (30-F11; BD Biosciences), and GP38 (AF3244; R&D Systems).

Image analysis of infiltrating leukocytes was performed using Aperio ImageScope software (Leica) and their Membrane Image Analysis algorithm to classify positive cells (+3) or by manual count (mast cells, F4/80+, and vessels) in blinded samples and enumerated per length of tissue. Number of cells per length from two sections of each ear were averaged. Epidermal and dermal thickness were determined through direct measurement of epidermis at five places along length of ear. Two sections of each ear were averaged. Lymphatic and blood vessel density was determined by manual count in blinded samples per length of tissue or as percent positive pixel area in more than representative regions of interest per sample.

Bone marrow chimeras
8–12-wk-old recipient mice received two doses of whole-body radiation (500 rads and 450 rads, 4 h apart) using an x-ray irradiator. Bone marrow was isolated from hind limbs of donor mice and $5–10 \times 10^6$ cells injected intravenously into recipients. Mice were maintained on 2 mg/ml Ampicillin (Fisher Bioreagents) antibiotic water changed twice per week for 6 wk. Mice were bled to check for efficient chimerism (>80%) and enrolled in studies 8 wk after radiation.

T cell activation and adoptive transfer
Spleens were passed through a 70-µm filter and lysed with ammonium-chloride-potassium lysis buffer. $5–6 \times 10^6$ splenocytes were plated in RPMI media (Gibco) supplemented with 10% FBS (Atlanta Biologicals) and 1% penicillin-streptomycin (Gibco). WT splenocytes were activated by plate-bound α-CD3 (10 µg/ml; 145-2C11; Tonbo) and α-CD28 (2 µg/ml; 37.51; eBioscience) supplemented with 100 U/ml IL-2 (Peprotech) for 72 h at 37°C. OT-I splenocytes were stimulated with SIINFEKL (1 nM; Biosynthesis) supplemented with 100 U/ml IL-2 for 72 h at 37°C. Alternatively, T cells were activated in vivo following transfer of naive CD8+ TCR-tg OT-I T cells into WT mice and infection 1 d later with 10^7 CFU attenuated WT LM or LM expressing the cognate antigens ovalbumin (LM-OVA). Spleens were harvested on day 7 after LM infection, passed through 70-µm pore filter (VWR) and red blood cells lysed with ammonium-chloride-potassium lysis buffer. CD8+ effector T cells were isolated using EasySep Mouse CD8+ T cell isolation kit (StemCell Technologies) according to manufactures instructions. 10^6 activated CD8+ T cells were transferred into tumor-bearing mice by intravenous injection.

LN digestion protocol
Cervical, inguinal, axillary, brachial, and mesenteric LNs were harvested into digestion buffer (DMEM-pyruvate [41965-062; Gibco], 1% penicillin/streptomycin, 1.2 mM $CaCl_2$, and 2% FBS, no β-mercaptoethanol) and capsule-teased apart with a 26-G needle. Single-cell suspensions were generated by sequential digestion with collagenase IV (220 U/ml) and DNase (>80 U/ml) followed by collagenase D (0.7854 U/ml) and DNase (>80 U/ml) as previously described (Lund et al., 2012; Hirosue et al., 2014).

TCGA
Upper-quartile normalized RNaseq by expectation maximization (RSEM) expected counts from the TCGA were taken from the Broad Institute Firehose and clinical variables taken from the UCSC Genome Browser. Non-glabrous melanoma samples ($n = 231$) representing primary cutaneous ($n = 103$), regional cutaneous metastases ($n = 74$), and distant metastasis ($n = 54$), but not regional LN metastases, were extracted and log-transformed for analysis. Scores were calculated as the first principal component of each gene set: LS, *VEGFC*, *LYVE1*, and *PDPN*; T cell inflammation score: *CD8A*, *CCL2*, *CCL3*, *CCL4*, *CXCL9*, *CXCL10*, *ICOS*, *GZMK*, *IRF1*, *HLA-DMA*, *HLA-DMB*, *HLA-DOA*, and *HLA-DOB* (Spranger et al., 2015); type II IFN score: *IFNI*, *STAT1*, *CCR5*, *CXCL9*, *PRF1*, *HLA-DRA*, *CXCL10*, *CXCL11*, *IDO1*, and *GZMA* (Ayers et al., 2017). LS was stratified to high and low cohorts LS^{lo} (< mean – 0.5 × SD; $n = 71$), LS^{hi} (> mean + 0.5 × SD; $n = 68$).

mIHC
Sequential chromogenic IHC was performed as previously described (Tsujikawa et al., 2017), using a modified protocol. In brief, 5-µm FFPE tissue sections of human primary melanoma were deparaffinized and subsequently stained with hematoxylin (GHS116; Sigma-Aldrich) to visualize nuclei. Following whole-tissue scanning using Aperio ImageScope AT (Leica Biosystems), heat-mediated antigen retrieval in antigen retrieval Citra Plus solution (HK080-9K; BioGenex) was performed. Subsequent iterative cycles of standard IHC were performed using primary antibodies against CD8 (C8/144B; Thermo Fisher Scientific) and CD31 (JC70A; Dako) or CD34 (QBEnd-10; Thermo Fisher Scientific), podoplanin (D2-40, Covance), and S100 (antibody cocktail; Biocare Medical), followed by detection with ImmPress IgG-polymerized peroxidase reagents (Vector Laboratories) and visualization with AEC (Vector Laboratories). After whole-tissue scanning, AEC was removed using ethanol, antibody was stripped in heated citrate buffer, and the next staining cycle with the next primary antibody was performed. Tissues were treated with 10% H_2O_2 (Fisher Chemical) for 10 min at 60°C immediately after deparaffinization to remove pigmentation.

Image processing
Serial digitized images were processed using a computational image analysis workflow described previously (Tsujikawa et al., 2017) to align and visualize several markers simultaneously in a single pseudo-colored image. From whole-tissue serial images, rectangular regions of interest (ROI) with an area of 6.25 mm² were selected based on quantitative analysis of CD8+ cell-density. One to three high-density CD8+ T cell ROIs that included both stromal tissue and tumor parenchyma were chosen from each patient sample for analysis. Images of nuclei, CD8, CD31 or CD34, podoplanin, and S100 staining were processed to obtain

quantitative and spatial information of staining intensity on a single-cell level and analyzed using FCS Express 5 Image Cytometry Version 5.01.0080 (De Novo Software).

Tumor segmentation masks to distinguish intratumoral and peritumoral regions were generated from the images of cell nuclei and the tumor marker S100 of the same tissue region. The segmentation pipeline is a succession of thresholding and mathematical morphology operations: first, the nuclei image is used to define the parts of the image covered by tissue using triangle thresholding. S100-positive areas are detected within the ROI by computing an alternate sequential filter (a succession of opening and closing with structuring elements of increasing sizes), followed by a triangle thresholding, and a cleaning with closing and opening operations which fill gaps and holes and remove artifacts to generate a black and white mask for the image region covered by tumor.

Vessel segmentation
Whole-vessel segmentation was performed using Otsu's method to segment blood and lymphatic vessels based on the intensity of $CD31^+$ or $CD34^+$ and podoplanin$^+$ staining. Blood vessels were defined as CD31 or CD34 single positive, and lymphatic vessel masks were generated using the intersection of masks generated from podoplanin staining with CD31 masks or when staining with CD34, from podoplanin staining alone. The segmentation masks were refined with morphological operation such as closing operation, i.e., dilation, followed by erosion using the same structuring element for both operations. Endothelial cell type was identified based on mIHC marker expression using image cytometry analysis, and vessel annotation was refined using the identified endothelial cell types and their location data; the image analysis output and threshold values from image cytometry were used to identify endothelial cells. The most frequent endothelial cell type within the individual segmented vessels was determined, and vessel type was reannotated based on the most frequent cell types in the segmented region. Finally, vessel segmentation and annotation was validated by visual assessment by an investigator to exclude objects falsely annotated as vessels due to unspecific staining, background, or errors in annotation overlooked by the automated procedure described above.

Extraction of spatial proximity and distance measurements
$CD8^+$ T cell positional data were used to measure distance from each individual T cell to the annotated vessels and tumor border. Using the Quickhull Algorithm for Convex Hulls, "dsearchn" function in MATLAB R2016, the shortest distance between T cell centroids and the boundary of the vessel segmentation mask was measured to determine T cell distance to vessels within peri- and intratumoral regions, respectively. Similarly, the shortest distance between T cell centroids or centroid of the vessels segmentation masks to the tumor border (boundary of the tumor tissue segmentation mask) were determined.

Statistical analysis
Statistical analyses were performed using GraphPad (Prism). In all cases, parametric or nonparametric Student's *t* test (two

groups) or one-way ANOVA for multiple pairwise testing (more than two groups) were performed as indicated. Changes in tumor growth were determined following approximation of linear regression and comparison of mean slope and variation. Analysis of survival was performed using Mantel-Cox test. $P < 0.05$ was considered significant in all studies, indicated by asterisks. All experiments were performed independently two to three times, and data were presented as cumulative or representative data as indicated. Details may be found in each figure legend.

Online supplemental material
Fig. S1 presents data demonstrating systemic role of hematopoietic PD-L1. Fig. S2 demonstrates PD-L1 expression in contralateral tissue sites. Fig. S3 provides control experiments demonstrating efficiency of the IFNγR Cre models. Fig. S4 demonstrates effects on LN lymphangiogenesis in IFNγR$^{-/-}$ models at steady-state and when draining sites of inflammation. Fig. S5 demonstrates in vivo Cre specificity. Table S1 provides demographic and clinical features for primary human melanoma cohort.

References

Alitalo, A.K., S.T. Proulx, S. Karaman, D. Aebischer, S. Martino, M. Jost, N. Schneider, M. Bry, and M. Detmar. 2013. VEGF-C and VEGF-D blockade inhibits inflammatory skin carcinogenesis. *Cancer Res.* 73:4212–4221. https://doi.org/10.1158/0008-5472.CAN-12-4539

Allan, R.S., J. Waithman, S. Bedoui, C.M. Jones, J.A. Villadangos, Y. Zhan, A.M. Lew, K. Shortman, W.R. Heath, and F.R. Carbone. 2006. Migratory dendritic cells transfer antigen to a lymph node-resident dendritic cell population for efficient CTL priming. *Immunity.* 25:153–162. https://doi.org/10.1016/j.immuni.2006.04.017

Ayers, M., J. Lunceford, M. Nebozhyn, E. Murphy, A. Loboda, D.R. Kaufman, A. Albright, J.D. Cheng, S.P. Kang, V. Shankaran, et al. 2017. IFN-γ-related mRNA profile predicts clinical response to PD-1 blockade. *J. Clin. Invest.* 127:2930–2940. https://doi.org/10.1172/JCI91190

Bedoui, S., P.G. Whitney, J. Waithman, L. Eidsmo, L. Wakim, I. Caminschi, R.S. Allan, M. Wojtasiak, K. Shortman, F.R. Carbone, et al. 2009. Cross-presentation of viral and self antigens by skin-derived CD103+ dendritic cells. *Nat. Immunol.* 10:488–495. https://doi.org/10.1038/ni.1724

Bordry, N., M.A.S. Broggi, K. de Jonge, K. Schaeuble, P.O. Gannon, P.G. Foukas, E. Danenberg, E. Romano, P. Baumgaertner, M. Fankhauser, et al. 2018. Lymphatic vessel density is associated with CD8+ T cell infiltration and immunosuppressive factors in human melanoma. *OncoImmunology.* 7:e1462878. https://doi.org/10.1080/2162402X.2018.1462878

Cannon, M.J., P.J.M. Openshaw, and B.A. Askonas. 1988. Cytotoxic T cells clear virus but augment lung pathology in mice infected with respiratory syncytial virus. *J. Exp. Med.* 168:1163–1168. https://doi.org/10.1084/jem.168.3.1163

Cohen, J.N., C.J. Guidi, E.F. Tewalt, H. Qiao, S.J. Rouhani, A. Ruddell, A.G. Farr, K.S. Tung, and V.H. Engelhard. 2010. Lymph node-resident lymphatic endothelial cells mediate peripheral tolerance via Aire-independent direct antigen presentation. *J. Exp. Med.* 207:681–688. https://doi.org/10.1084/jem.20092465

Cohen, J.N., E.F. Tewalt, S.J. Rouhani, E.L. Buonomo, A.N. Bruce, X. Xu, S. Bekiranov, Y.X. Fu, and V.H. Engelhard. 2014. Tolerogenic properties of lymphatic endothelial cells are controlled by the lymph node microenvironment. *PLoS One.* 9:e87740. https://doi.org/10.1371/journal.pone.0087740

Creagan, E.T., C.L. Loprinzi, D.L. Ahmann, and D.J. Schaid. 1988. A phase I-II trial of the combination of recombinant leukocyte A interferon and recombinant human interferon-gamma in patients with metastatic malignant melanoma. *Cancer.* 62:2472–2474. https://doi.org/10.1002/1097-0142(19881215)62:12%3C2472::AID-CNCR2820621203%3E3.0.CO;2-G

Dieterich, L.C., K. Ikenberg, T. Cetintas, K. Kapaklikaya, C. Hutmacher, and M. Detmar. 2017. Tumor-Associated Lymphatic Vessels Upregulate PDL1 to Inhibit T-Cell Activation. *Front. Immunol.* 8:66. https://doi.org/10.3389/fimmu.2017.00066

El Annan, J., S. Goyal, Q. Zhang, G.J. Freeman, A.H. Sharpe, and R. Dana. 2010. Regulation of T-cell chemotaxis by programmed death-ligand 1 (PD-L1) in dry eye-associated corneal inflammation. *Invest. Ophthalmol. Vis. Sci.* 51:3418–3423. https://doi.org/10.1167/iovs.09-3684

Fankhauser, M., M.A.S. Broggi, L. Potin, N. Bordry, L. Jeanbart, A.W. Lund, E. Da Costa, S. Hauert, M. Rincon-Restrepo, C. Tremblay, et al. 2017. Tumor lymphangiogenesis promotes T cell infiltration and potentiates immunotherapy in melanoma. *Sci. Transl. Med.* 9:eaal4712. https://doi.org/10.1126/scitranslmed.aal4712

Fonseca, D.M., T.W. Hand, S.J. Han, M.Y. Gerner, A. Glatman Zaretsky, A.L. Byrd, O.J. Harrison, A.M. Ortiz, M. Quinones, G. Trinchieri, et al. 2015. Microbiota-Dependent Sequelae of Acute Infection Compromise Tissue-Specific Immunity. *Cell.* 163:354–366. https://doi.org/10.1016/j.cell.2015.08.030

Frebel, H., V. Nindl, R.A. Schuepbach, T. Braunschweiler, K. Richter, J. Vogel, C.A. Wagner, D. Loffing-Cueni, M. Kurrer, B. Ludewig, and A. Oxenius. 2012. Programmed death 1 protects from fatal circulatory failure during systemic virus infection of mice. *J. Exp. Med.* 209:2485–2499. https://doi.org/10.1084/jem.20121015

Garcia-Diaz, A., D.S. Shin, B.H. Moreno, J. Saco, H. Escuin-Ordinas, G.A. Rodriguez, J.M. Zaretsky, L. Sun, W. Hugo, X. Wang, et al. 2017. Interferon Receptor Signaling Pathways Regulating PD-L1 and PD-L2 Expression. *Cell Reports.* 19:1189–1201. https://doi.org/10.1016/j.celrep.2017.04.031

Herbst, R.S., J.C. Soria, M. Kowanetz, G.D. Fine, O. Hamid, M.S. Gordon, J.A. Sosman, D.F. McDermott, J.D. Powderly, S.N. Gettinger, et al. 2014. Predictive correlates of response to the anti-PD-L1 antibody MPDL3280A in cancer patients. *Nature.* 515:563–567. https://doi.org/10.1038/nature14011

Hickman, H.D., G.V. Reynoso, B.F. Ngudiankama, E.J. Rubin, J.G. Magadán, S.S. Cush, J. Gibbs, B. Molon, V. Bronte, J.R. Bennink, and J.W. Yewdell. 2013. Anatomically restricted synergistic antiviral activities of innate and adaptive immune cells in the skin. *Cell Host Microbe.* 13:155–168. https://doi.org/10.1016/j.chom.2013.01.004

Hirosue, S., E. Vokali, V.R. Raghavan, M. Rincon-Restrepo, A.W. Lund, P. Corthésy-Henrioud, F. Capotosti, C. Halin Winter, S. Hugues, and M.A. Swartz. 2014. Steady-state antigen scavenging, cross-presentation, and CD8+ T cell priming: a new role for lymphatic endothelial cells. *J. Immunol.* 192:5002–5011. https://doi.org/10.4049/jimmunol.1302492

Hoves, S., C.H. Ooi, C. Wolter, H. Sade, S. Bissinger, M. Schmittnaegel, O. Ast, A.M. Giusti, K. Wartha, V. Runza, et al. 2018. Rapid activation of tumor-associated macrophages boosts preexisting tumor immunity. *J. Exp. Med.* 215:859–876. https://doi.org/10.1084/jem.20171440

Ikeda, H., L.J. Old, and R.D. Schreiber. 2002. The roles of IFN gamma in protection against tumor development and cancer immunoediting. *Cytokine Growth Factor Rev.* 13:95–109. https://doi.org/10.1016/S1359-6101(01)00038-7

Johnson, L.A., S. Clasper, A.P. Holt, P.F. Lalor, D. Baban, and D.G. Jackson. 2006. An inflammation-induced mechanism for leukocyte transmigration across lymphatic vessel endothelium. *J. Exp. Med.* 203:2763–2777. https://doi.org/10.1084/jem.20051759

Johnson, L.A., R. Prevo, S. Clasper, and D.G. Jackson. 2007. Inflammation-induced uptake and degradation of the lymphatic endothelial hyaluronan receptor LYVE-1. *J. Biol. Chem.* 282:33671–33680. https://doi.org/10.1074/jbc.M702889200

Johnson, L.A., S. Banerji, W. Lawrance, U. Gileadi, G. Prota, K.A. Holder, Y.M. Roshorm, T. Hanke, V. Cerundolo, N.W. Gale, and D.G. Jackson. 2017. Dendritic cells enter lymph vessels by hyaluronan-mediated docking to the endothelial receptor LYVE-1. *Nat. Immunol.* 18:762–770. https://doi.org/10.1038/ni.3750

Juneja, V.R., K.A. McGuire, R.T. Manguso, M.W. LaFleur, N. Collins, W.N. Haining, G.J. Freeman, and A.H. Sharpe. 2017. PD-L1 on tumor cells is sufficient for immune evasion in immunogenic tumors and inhibits CD8 T cell cytotoxicity. *J. Exp. Med.* 214:895–904. https://doi.org/10.1084/jem.20160801

Kataru, R.P., H. Kim, C. Jang, D.K. Choi, B.I. Koh, M. Kim, S. Gollamudi, Y.K. Kim, S.H. Lee, and G.Y. Koh. 2011. T lymphocytes negatively regulate lymph node lymphatic vessel formation. *Immunity.* 34:96–107. https://doi.org/10.1016/j.immuni.2010.12.016

Kleffel, S., C. Posch, S.R. Barthel, H. Mueller, C. Schlapbach, E. Guenova, C.P. Elco, N. Lee, V.R. Juneja, Q. Zhan, et al. 2015. Melanoma Cell-Intrinsic PD-1 Receptor Functions Promote Tumor Growth. *Cell.* 162:1242–1256. https://doi.org/10.1016/j.cell.2015.08.052

Lin, H., S. Wei, E.M. Hurt, M.D. Green, L. Zhao, L. Vatan, W. Szeliga, R. Herbst, P.W. Harms, L.A. Fecher, et al. 2018. Host expression of PD-L1 determines efficacy of PD-L1 pathway blockade-mediated tumor regression. *J. Clin. Invest.* 128:805–815. https://doi.org/10.1172/JCI96113

Loo, C.P., N.A. Nelson, R.S. Lane, J.L. Booth, S.C. Loprinzi Hardin, A. Thomas, M.K. Slifka, J.C. Nolz, and A.W. Lund. 2017. Lymphatic Vessels Balance Viral Dissemination and Immune Activation following Cutaneous Viral Infection. *Cell Reports.* 20:3176–3187. https://doi.org/10.1016/j.celrep.2017.09.006

Lucas, E.D., J.M. Finlon, M.A. Burchill, M.K. McCarthy, T.E. Morrison, T.M. Colpitts, and B.A.J. Tamburini. 2018. Type 1 IFN and PD-L1 Coordinate Lymphatic Endothelial Cell Expansion and Contraction during an Inflammatory Immune Response. *J. Immunol.* 201:1735–1747. https://doi.org/10.4049/jimmunol.1800271

Lukacs-Kornek, V., D. Malhotra, A.L. Fletcher, S.E. Acton, K.G. Elpek, P. Tayalia, A.R. Collier, and S.J. Turley. 2011. Regulated release of nitric oxide by nonhematopoietic stroma controls expansion of the activated T cell pool in lymph nodes. *Nat. Immunol.* 12:1096–1104. https://doi.org/10.1038/ni.2112

Lund, A.W. 2016. Rethinking Lymphatic Vessels and Antitumor Immunity. *Trends Cancer.* 2:548–551. https://doi.org/10.1016/j.trecan.2016.09.005

Lund, A.W., F.V. Duraes, S. Hirosue, V.R. Raghavan, C. Nembrini, S.N. Thomas, A. Issa, S. Hugues, and M.A. Swartz. 2012. VEGF-C promotes immune tolerance in B16 melanomas and cross-presentation of tumor antigen by lymph node lymphatics. *Cell Reports.* 1:191–199. https://doi.org/10.1016/j.celrep.2012.01.005

Lund, A.W., T.R. Medler, S.A. Leachman, and L.M. Coussens. 2016a. Lymphatic Vessels, Inflammation, and Immunity in Skin Cancer. *Cancer Discov.* 6:22–35. https://doi.org/10.1158/2159-8290.CD-15-0023

Lund, A.W., M. Wagner, M. Fankhauser, E.S. Steinskog, M.A. Broggi, S. Spranger, T.F. Gajewski, K. Alitalo, H.P. Eikesdal, H. Wiig, and M.A. Swartz. 2016b. Lymphatic vessels regulate immune microenvironments in human and murine melanoma. *J. Clin. Invest.* 126:3389–3402. https://doi.org/10.1172/JCI79434

Meeth, K., J.X. Wang, G. Micevic, W. Damsky, and M.W. Bosenberg. 2016. The YUMM lines: a series of congenic mouse melanoma cell lines with defined genetic alterations. *Pigment Cell Melanoma Res.* 29:590–597. https://doi.org/10.1111/pcmr.12498

Miteva, D.O., J.M. Rutkowski, J.B. Dixon, W. Kilarski, J.D. Shields, and M.A. Swartz. 2010. Transmural flow modulates cell and fluid transport functions of lymphatic endothelium. *Circ. Res.* 106:920–931. https://doi.org/10.1161/CIRCRESAHA.109.207274

Mlecnik, B., G. Bindea, A. Kirilovsky, H.K. Angell, A.C. Obenauf, M. Tosolini, S.E. Church, P. Maby, A. Vasaturo, M. Angelova, et al. 2016. The tumor microenvironment and Immunoscore are critical determinants of dissemination to distant metastasis. *Sci. Transl. Med.* 8:327ra26. https://doi.org/10.1126/scitranslmed.aad6352

Mueller, S.N., V.K. Vanguri, S.J. Ha, E.E. West, M.E. Keir, J.N. Glickman, A.H. Sharpe, and R. Ahmed. 2010. PD-L1 has distinct functions in hematopoietic and nonhematopoietic cells in regulating T cell responses during chronic infection in mice. *J. Clin. Invest.* 120:2508–2515. https://doi.org/10.1172/JCI40040

Nirschl, C.J., M. Suárez-Fariñas, B. Izar, S. Prakadan, R. Dannenfelser, I. Tirosh, Y. Liu, Q. Zhu, K.S.P. Devi, S.L. Carroll, et al. 2017. IFNγ-Dependent Tissue-Immune Homeostasis Is Co-opted in the Tumor Microenvironment. *Cell.* 170:127–141.e15. https://doi.org/10.1016/j.cell.2017.06.016

Nolz, J.C., and J.T. Harty. 2014. IL-15 regulates memory CD8+ T cell O-glycan synthesis and affects trafficking. *J. Clin. Invest.* 124:1013–1026. https://doi.org/10.1172/JCI72039

Osanto, S., R. Jansen, A.M.I.H. Naipal, J.W. Gratama, A. van Leeuwen, and F.J. Cleton. 1989. In vivo effects of combination treatment with recombinant interferon-gamma and -alpha in metastatic melanoma. *Int. J. Cancer.* 43:1001–1006. https://doi.org/10.1002/ijc.2910430608

Pan, W., S. Zhu, K. Qu, K. Meeth, J. Cheng, K. He, H. Ma, Y. Liao, X. Wen, C. Roden, et al. 2017. The DNA Methylcytosine Dioxygenase Tet2 Sustains Immunosuppressive Function of Tumor-Infiltrating Myeloid Cells to Promote Melanoma Progression. *Immunity.* 47:284–297.e5. https://doi.org/10.1016/j.immuni.2017.07.020

Pasquali, S., A.P. van der Ploeg, S. Mocellin, J.R. Stretch, J.F. Thompson, and R.A. Scolyer. 2013. Lymphatic biomarkers in primary melanomas as predictors of regional lymph node metastasis and patient outcomes. *Pigment Cell Melanoma Res.* 26:326–337. https://doi.org/10.1111/pcmr.12064

Pauken, K.E., M.K. Jenkins, M. Azuma, and B.T. Fife. 2013. PD-1, but not PD-L1, expressed by islet-reactive CD4+ T cells suppresses infiltration of the pancreas during type 1 diabetes. *Diabetes.* 62:2859–2869. https://doi.org/10.2337/db12-1475

Perry, C.J., A.R. Muñoz-Rojas, K.M. Meeth, L.N. Kellman, R.A. Amezquita, D. Thakral, V.Y. Du, J.X. Wang, W. Damsky, A.L. Kuhlmann, et al. 2018. Myeloid-targeted immunotherapies act in synergy to induce inflammation and antitumor immunity. *J. Exp. Med.* 215:877–893. https://doi.org/10.1084/jem.20171435

Pittet, C.L., J. Newcombe, A. Prat, and N. Arbour. 2011. Human brain endothelial cells endeavor to immunoregulate CD8 T cells via PD-1 ligand expression in multiple sclerosis. *J. Neuroinflammation.* 8:155. https://doi.org/10.1186/1742-2094-8-155

Reuben, A., C.N. Spencer, P.A. Prieto, V. Gopalakrishnan, S.M. Reddy, J.P. Miller, X. Mao, M.P. De Macedo, J. Chen, X. Song, et al. 2017. Genomic and immune heterogeneity are associated with differential responses to therapy in melanoma. *NPJ Genom. Med.* 2:10. https://doi.org/10.1038/s41525-017-0013-8

Ribas, A. 2015. Adaptive Immune Resistance: How Cancer Protects from Immune Attack. *Cancer Discov.* 5:915–919. https://doi.org/10.1158/2159-8290.CD-15-0563

Ribas, A., O. Hamid, A. Daud, F.S. Hodi, J.D. Wolchok, R. Kefford, A.M. Joshua, A. Patnaik, W.J. Hwu, J.S. Weber, et al. 2016. Association of Pembrolizumab With Tumor Response and Survival Among Patients With Advanced Melanoma. *JAMA.* 315:1600–1609. https://doi.org/10.1001/jama.2016.4059

Robert, C., J. Schachter, G.V. Long, A. Arance, J.J. Grob, L. Mortier, A. Daud, M.S. Carlino, C. McNeil, M. Lotem, et al. KEYNOTE-006 investigators. 2015. Pembrolizumab versus Ipilimumab in Advanced Melanoma. *N. Engl. J. Med.* 372:2521–2532. https://doi.org/10.1056/NEJMoa1503093

Roberts, E.W., M.L. Broz, M. Binnewies, M.B. Headley, A.E. Nelson, D.M. Wolf, T. Kaisho, D. Bogunovic, N. Bhardwaj, and M.F. Krummel. 2016. Critical Role for CD103(+)/CD141(+) Dendritic Cells Bearing CCR7 for Tumor Antigen Trafficking and Priming of T Cell Immunity in Melanoma. *Cancer Cell.* 30:324–336. https://doi.org/10.1016/j.ccell.2016.06.003

Rohner, N.A., J. McClain, S.L. Tuell, A. Warner, B. Smith, Y. Yun, A. Mohan, M. Sushnitha, and S.N. Thomas. 2015. Lymph node biophysical remodeling is associated with melanoma lymphatic drainage. *FASEB J.* 29:4512–4522. https://doi.org/10.1096/fj.15-274761

Rouhani, S.J., J.D. Eccles, P. Riccardi, J.D. Peske, E.F. Tewalt, J.N. Cohen, R. Liblau, T. Mäkinen, and V.H. Engelhard. 2015. Roles of lymphatic endothelial cells expressing peripheral tissue antigens in CD4 T-cell tolerance induction. *Nat. Commun.* 6:6771. https://doi.org/10.1038/ncomms7771

Ruddell, A., S.B. Kirschbaum, S.N. Ganti, C.L. Liu, R.R. Sun, and S.C. Partridge. 2015. Tumor-induced alterations in lymph node lymph drainage identified by contrast-enhanced MRI. *J. Magn. Reson. Imaging.* 42:145–152. https://doi.org/10.1002/jmri.24754

Scandiuzzi, L., K. Ghosh, K.A. Hofmeyer, Y.M. Abadi, E. Lázár-Molnár, E.Y. Lin, Q. Liu, H. Jeon, S.C. Almo, L. Chen, et al. 2014. Tissue-expressed B7-H1 critically controls intestinal inflammation. *Cell Reports.* 6:625–632. https://doi.org/10.1016/j.celrep.2014.01.020

Schmittnaegel, M., N. Rigamonti, E. Kadioglu, A. Cassará, C. Wyser Rmili, A. Kiialainen, Y. Kienast, H.J. Mueller, C.H. Ooi, D. Laoui, and M. De Palma. 2017. Dual angiopoietin-2 and VEGFA inhibition elicits antitumor immunity that is enhanced by PD-1 checkpoint blockade. *Sci. Transl. Med.* 9:eaak9670. https://doi.org/10.1126/scitranslmed.aak9670

Skobe, M., T. Hawighorst, D.G. Jackson, R. Prevo, L. Janes, P. Velasco, L. Riccardi, K. Alitalo, K. Claffey, and M. Detmar. 2001. Induction of tumor lymphangiogenesis by VEGF-C promotes breast cancer metastasis. *Nat. Med.* 7:192–198. https://doi.org/10.1038/84643

Spranger, S., R.M. Spaapen, Y. Zha, J. Williams, Y. Meng, T.T. Ha, and T.F. Gajewski. 2013. Up-regulation of PD-L1, IDO, and T(regs) in the melanoma tumor microenvironment is driven by CD8(+) T cells. *Sci. Transl. Med.* 5:200ra116. https://doi.org/10.1126/scitranslmed.3006504

Spranger, S., R. Bao, and T.F. Gajewski. 2015. Melanoma-intrinsic β-catenin signalling prevents anti-tumour immunity. *Nature.* 523:231–235. https://doi.org/10.1038/nature14404

Stacker, S.A., S.P. Williams, T. Karnezis, R. Shayan, S.B. Fox, and M.G. Achen. 2014. Lymphangiogenesis and lymphatic vessel remodelling in cancer. *Nat. Rev. Cancer.* 14:159–172. https://doi.org/10.1038/nrc3677

Tamburini, B.A., M.A. Burchill, and R.M. Kedl. 2014. Antigen capture and archiving by lymphatic endothelial cells following vaccination or viral infection. *Nat. Commun.* 5:3989. https://doi.org/10.1038/ncomms4989

Tang, H., Y. Liang, R.A. Anders, J.M. Taube, X. Qiu, A. Mulgaonkar, X. Liu, S.M. Harrington, J. Guo, Y. Xin, et al. 2018. PD-L1 on host cells is essential for PD-L1 blockade-mediated tumor regression. *J. Clin. Invest.* 128:580–588. https://doi.org/10.1172/JCI96061

Tewalt, E.F., J.N. Cohen, S.J. Rouhani, C.J. Guidi, H. Qiao, S.P. Fahl, M.R. Conaway, T.P. Bender, K.S. Tung, A.T. Vella, et al. 2012. Lymphatic endothelial cells induce tolerance via PD-L1 and lack of costimulation leading to high-level PD-1 expression on CD8 T cells. *Blood.* 120:4772–4782. https://doi.org/10.1182/blood-2012-04-427013

Topalian, S.L., F.S. Hodi, J.R. Brahmer, S.N. Gettinger, D.C. Smith, D.F. McDermott, J.D. Powderly, R.D. Carvajal, J.A. Sosman, M.B. Atkins, et al. 2012. Safety, activity, and immune correlates of anti-PD-1 antibody in cancer. *N. Engl. J. Med.* 366:2443–2454. https://doi.org/10.1056/NEJMoa1200690

Tsujikawa, T., S. Kumar, R.N. Borkar, V. Azimi, G. Thibault, Y.H. Chang, A. Balter, R. Kawashima, G. Choe, D. Sauer, et al. 2017. Quantitative Multiplex Immunohistochemistry Reveals Myeloid-Inflamed Tumor-Immune Complexity Associated with Poor Prognosis. *Cell Reports.* 19:203–217. https://doi.org/10.1016/j.celrep.2017.03.037

Vigl, B., D. Aebischer, M. Nitschké, M. Iolyeva, T. Röthlin, O. Antsiferova, and C. Halin. 2011. Tissue inflammation modulates gene expression of lymphatic endothelial cells and dendritic cell migration in a stimulus-dependent manner. *Blood.* 118:205–215. https://doi.org/10.1182/blood-2010-12-326447

Wang, J., C.J. Perry, K. Meeth, D. Thakral, W. Damsky, G. Micevic, S. Kaech, K. Blenman, and M. Bosenberg. 2017. UV-induced somatic mutations elicit a functional T cell response in the YUMMER1.7 mouse melanoma model. *Pigment Cell Melanoma Res.* 30:428–435. https://doi.org/10.1111/pcmr.12591

Wolchok, J.D., H. Kluger, M.K. Callahan, M.A. Postow, N.A. Rizvi, A.M. Lesokhin, N.H. Segal, C.E. Ariyan, R.A. Gordon, K. Reed, et al. 2013. Nivolumab plus ipilimumab in advanced melanoma. *N. Engl. J. Med.* 369:122–133. https://doi.org/10.1056/NEJMoa1302369